Global Systematics of Mid-Ocean Ridge Morphology

Christopher Small

Lamont-Doherty Earth Observatory, Columbia University, Palisades, NY

Global mid-ocean ridge morphology is characterized by a dichotomy in which slow spreading centers have discontinuous axial valleys and rugged flanking morphology while fast spreading centers have more continuous axial rises and smoother flanking morphology. This study investigates the relationship between axial and flanking morphology and the nature of the dichotomy. Both axial and flanking morphology show similar variations with spreading rate but the transition between axial valley and axial rise morphology suggests that the amplitude of the axial morphology is not the sole determinant of flanking roughness. At slower spreading rates, ridge flank roughness is moderately correlated with axial valley relief, but at intermediate spreading rates significant seafloor deformation can occur without the formation of an axial rise or axial valley. At faster spreading rates, well developed axial rises have smoother flanking morphology and show no correlation between axial relief and flanking roughness. This reflects a fundamental difference in the mechanisms of lithospheric deformation as well as the importance of extrusive volcanism at high spreading rates and thermal environments where an axial magma chamber can be maintained. Axial valley spreading centers exhibit a spreading rate dependence in both amplitude and variability of axial relief, asymmetry, flanking roughness and depth but spreading centers with axial rises show much less variability and no spreading rate dependence for any observable above intermediate (~70 km/Ma) spreading rates. The variability of axial valley environments at a given spreading rate results primarily from intrasegment structure but may also reflect temporal episodicity of magmatic emplacement and extension. The dichotomy, which is also manifest in the subsurface structure of spreading centers, suggests a transition from episodicity and rate dependence at slow spreading rates to a metastable mode of lithospheric accretion at faster spreading rates. The most plausible mechanism for the transition is a stabilization of mid-ocean ridge thermal structure above a critical spreading rate.

INTRODUCTION

Bathymetric measurements at mid-ocean ridges provide three complementary types of information: the actual depth below sea level, the characteristic axial morphology and the smaller scale roughness superimposed on the axis and ridge flanks. The relationships between the different components of morphology are controlled by the processes that form and deform the lithosphere. The tectonic complexity of most ridge flanks precludes simple generalizations relating axial and flanking morphology but global patterns are observed in both types of morphology. The global systematics of these patterns reveal a structure to the system that is not always obvious in studies of individual spreading centers.

Faulting and Magmatism at Mid-Ocean Ridges
Geophysical Monograph 106

Until recently, our understanding of mid-ocean ridges was based almost entirely on detailed studies of the northern Mid-Atlantic Ridge and the northern East Pacific Rise. These spreading centers conveniently characterize the diverse end members of the global system and offer complementary views of the processes of lithospheric accretion, but to understand how these processes operate globally it is necessary to consider the entire system of mid-ocean ridges. By investigating the relationship between the consistently observed characteristic features of mid-ocean ridges and the variability in the morphology that changes from one location to the another it may be possible to better understand the dynamics of the entire system. The purpose of this study is to quantify the global systematics and to provide constraints on the processes of lithospheric deformation at mid-ocean ridge plate boundaries.

One of the earliest observations of seafloor structure was a dichotomy between the axial morphology of the Mid-Atlantic Ridge and the East Pacific Rise [*Heezen,* 1960, *Menard,* 1960]. Further exploration of the global system revealed that slow spreading mid-ocean ridges are generally characterized by deep axial valleys and uplifted flanks while faster spreading mid-ocean ridges have narrow axial rises [e.g. *Macdonald,* 1982]. It was shown by *Macdonald* [1986] that the relief of axial valleys tends to diminish with increasing spreading rate and *Small and Sandwell* [1989] showed that this spreading rate dependence of axial valley structure is contrasted by an insensitivity of axial rise structure to changes in spreading rate. The dichotomy in axial morphology has prompted extensive modeling efforts directed at understanding the spreading rate dependence of ridge axis dynamics (see *Poliakov and Buck* [*this volume*] for a review) but less attention has been paid to the actual transition from one morphology to the other. This is largely a result of the fact that most of the intermediate spreading rate ridges that characterize this transition had not been adequately surveyed until recently.

In addition to the dichotomy in axial morphology, it has been similarly observed that the flanking seafloor created at slow spreading centers is generally more rugged than that created at fast spreading centers [*Menard,* 1967]. Previous analyses of seafloor "roughness" have attempted to quantify this observation but reach no consensus as to whether the spreading rate dependence is discontinuous [*Small et al* 1989], a power law [*Malinverno,* 1991], or linear [*Hayes and Kane* 1991]. The distinction is important because it places a fundamental constraint on the processes that create the morphology of the seafloor and how these processes operate on a global scale. Over long time scales, seafloor roughness is strongly affected by migration of ridge axis offsets and off-axis volcanism but stochastic analyses of multibeam bathymetry [e.g. *Goff,* 1991; *Goff et al,* 1997] suggest that some characteristics of abyssal hill morphology vary with spreading rate. The apparent correlation between ridge axis morphology and ridge flank roughness suggests a causal relationship between the two.

Variations in mid-ocean ridge dynamics and structure are generally discussed with respect to spreading rate but "anomalous" spreading centers such as the Reykjanes Ridge and the Australian Antarctic Discordance (AAD) suggest that these variations are not dependent strictly on spreading rate but rather on temperature. Mid-ocean ridges are often parameterized by spreading rate because it kinematically exerts a first order control on both the rate of deformation and the regional thermal structure of the plate boundary. Spreading rate is also one of the few controlling parameters of mid-ocean ridge dynamics that can be accurately determined on a global basis.

This study establishes global systematics for spreading center depth, axial morphology, and near axis topographic roughness using a collection of 228 bathymetric profiles from the global mid-ocean ridge system (Figure 1). Spreading center depths discussed in this study include both zero-age depth and mean profile depth. When referring to axial morphology, profiles on which the zero-age depth is greater than the mean profile depth will be categorized as axial valleys and the term axial rise will be used for profiles on which the zero-age depth is less than the mean profile depth. The finer scale morphology of the ridge axis and flanks, referred to here as roughness, will be described statistically as discussed below.

The justification for using profile data is the widespread availability over the global mid-ocean ridge system which is not yet available from multibeam and sidescan sonar datasets. The trade-off is between local detail and global coverage. A number of studies have used the two dimensional coverage offered by multibeam swath bathymetry data and sidescan sonar imagery to study specific processes such as segmentation evolution [e.g. *Carbotte et al,* 1991; *Gente et al.* 1992]. and abyssal hill formation [e.g. *Goff and Jordan,* 1988; *Edwards et al,* 1991; *Goff,* 1991] but profile data can provide a complementary global view of the system. Studies based on profile data alone should however be interpreted in light of more detailed local studies. A global analysis of profile data may establish the first order relationships between axial and flanking morphology to which more detailed local studies may be related.

SEAFLOOR ROUGHNESS AND LITHOSPHERIC DEFORMATION

Mechanisms

In general, the morphology of a mid-ocean ridge flank results from a combination of abyssal hills, volcanic edifices and scars left by migrating offsets of the ridge axis. Both offset propagation [e.g. *Hey et al,* 1977; *Macdonald,* 1988] and seamount production [e.g. *Batiza,* 1982; *Epp and Smoot,* 1989] are widespread and appear to be influenced by spreading rate, but neither process is as ubiquitous as abyssal hill formation. The creation of

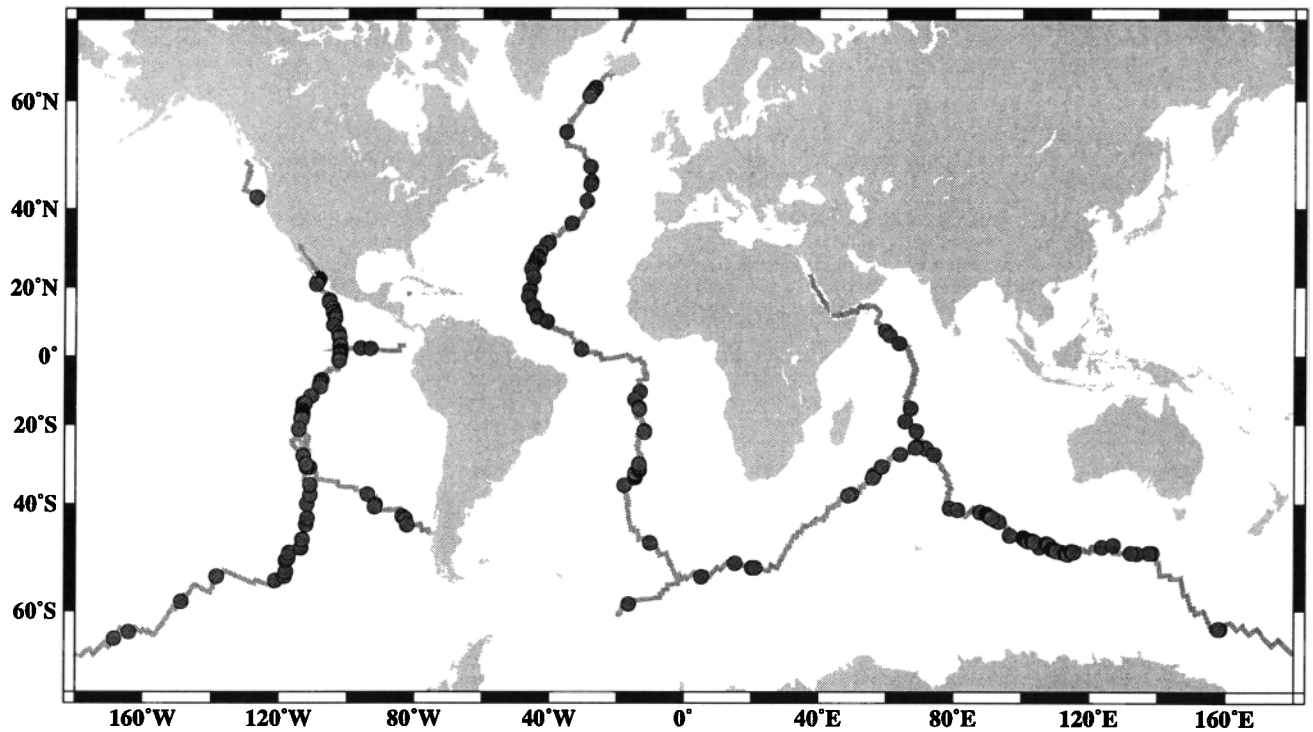

Figure 1. The global mid-ocean ridge system and the geographic distribution of the 228 bathymetric profiles used in this study. All profiles extend at least 40 km on each side of the ridge, cross the ridge within 45° of perpendicular and do not intersect known transforms or fracture zones.

abyssal hills at spreading centers with axial valleys is dominated by faulting [e.g. *Macdonald and Atwater,* 1978; *Macdonald,* 1982; *Shaw and Lin,* 1993] while abyssal hills formed near axial rises are believed to result from a combination of faulting and constructional volcanism [e.g. *Lonsdale,* 1977; *Lewis,* 1979; *Macdonald and Luyendyk,* 1985; *Macdonald et al,* 1996]. It is often assumed that there is a genetic relationship between the ridge flank roughness and the morphology of the spreading center at the time the flanking lithosphere was created [e.g. *Marks and Stock,* 1994; *Sahabi et al,* 1996]. This assumption is impossible to test since current rates of plate motion preclude direct observation of the movement of axial lithosphere to the ridge flank. It is however possible to systematically investigate the relationship between present day axial morphology and near axis roughness in order to understand how axial morphology contributes to lithospheric deformation.

Along axis migration of spreading center offsets also contributes to ridge flank roughness. In past studies, ridge flank roughness has often been assumed to be synonymous with abyssal hill topography but recognition of the importance of small offset propagation [*Macdonald,* 1988; *Carbotte et al.,* 1991; *Grindlay et al.,* 1991] suggests that some fraction of the topographic relief on ridge flanks is related to scars left by migration of axial discontinuities throughout the history of the ridge segment. Propagation of an offset through ridge flank lithosphere generally produces pseudofaults that are distinct from abyssal hills in both their amplitude and orientation and may represent different deformational mechanisms than those forming abyssal hills at the ridge axis. Detailed ridge flank surveys [e.g. *Gente et al,* 1992; *Tucholke et al,* 1997] reveal that, in addition to the smaller scale abyssal hill topography, there is a larger scale pattern of semi-continuous deeps amid larger (10's of kms) shoals. The continuity of the deeps, and their relation to present day segmentation, suggests that they are created by migrating offsets. Since the majority of ridge axis offsets are shorter than 40 km [*Ludwig and Small,* 1997], it can be inferred that the lithosphere into which the offsets propagate is relatively young but not necessarily within the neovolcanic zone. Thus, the roughness observed on the ridge flanks results from a combination of two distinct types of deformation in addition to some component of constructional volcanism.

Seamount volcanism also contributes to the ridge flank morphology but the variation in roughness discussed here is probably dominated by abyssal hills and propagating offsets. Studies of seamount populations in the Atlantic Ocean indicate that off axis constructional volcanism

(seamounts >100 m high) is generally related to hotspots [*Epp and Smoot,* 1989] and that seamounts formed near the axis of slow spreading centers are generally smaller (< 150 m, [*Smith and Cann,* 1992]) than the average abyssal hill height (>140 m, [*Goff et al,* 1995]). Seamounts formed near axial rises tend to be larger than the surrounding abyssal hills but cover only a small percentage of the seafloor. *Scheirer and Macdonald* [1995] find that near axis seamounts on the EPR (8°N - 17°N) have a characteristic height of 240 m but cover only ~6% of the surveyed seafloor. These observations of seamount abundance suggest that constructional volcanic edifices have a negligible effect on the average roughness of the seafloor formed at axial rises.

Controlling Parameters

If near-axis flanking morphology results primarily from the deformational processes at the ridge axis then we might expect the form and relief of the axial morphology to affect the roughness of the seafloor created there. The physical process of moving lithosphere from the axis of a spreading center to the flanks requires that it traverse the axial morphology and suggests that it is deformed in the process. Similarly, the morphology of propagating offsets also appears to be related to the axial morphology of the spreading center [e.g. *Macdonald et al,* 1988; *Gente et al,* 1992]. It stands to reason that the morphology of the ridge flanks may be related to the form and relief of the axial morphology. The degree of correlation between the present day axial morphology and recently created flanking morphology may provide a constraint on the degree of temporal variability of axial morphology and the extent to which ridge crest morphology is a steady state feature of the plate boundary. Temporal variations in the mechanism(s) that create axial topography may result in spatial variations in flanking roughness thereby weakening any global correlation between present day morphology and time averaged roughness; a strong correlation would suggest otherwise.

The roughness of near axis flanking topography should be controlled, in part, by the extensional strength of the lithosphere. Stronger lithosphere will withstand greater stress before undergoing brittle failure [e.g. *Huang and Solomon,* 1988], thereby creating and maintaining greater relief than weaker lithosphere. Extensional strength of the lithosphere is modulated by both temperature and crustal thickness. Higher temperatures at the ridge axis weaken lithosphere by reducing its ductile yield strength [e.g. *Brace and Kohlstedt,* 1980], but also by producing thicker crust [e.g. *Klein and Langmuir,* 1987]. Since oceanic crust is rheologically weaker than oceanic mantle, the net effect of crustal thickening is to reduce the overall strength of the lithosphere. Oceanic lithosphere strengthens monotonically with age as a result of cooling [*McNutt and Menard,* 1982] but the difference in crust and mantle rheologies delays rapid strengthening until the mantle has cooled sufficiently to undergo brittle deformation. The combined effect of the strengthening with age and the basal stress field on the plate is to concentrate lithospheric deformation in the area near the ridge axis [*Tapponier and Francheteau,* 1978; *Lin and Parmentier,* 1989; *Chen and Morgan,* 1990*a,b*]. This is consistent with the observation that abyssal hills are formed within several kilometers of the ridge axis [*Le Pichon,* 1969; *Edwards et al,* 1991].

Variations in lithospheric strength also result from along-axis differences in temperature and crustal thickness related to ridge segmentation. Detailed studies of the northern Mid-Atlantic Ridge [*Shaw,* 1992; *Shaw and Lin,* 1993; *Tucholke and Lin,* 1994; *Goff et al,* 1995; *Shaw and Lin,* 1996] highlight the importance of intra-segment variations in lithospheric strength to deformation within the axial valley. Studies on the East Pacific Rise [*Goff et al,* 1991; *Carbotte and Macdonald,* 1994b] also find intra-segment variations in abyssal hill morphology and tectonic fabric at axial rise spreading centers.

Higher temperatures and thicker crust conspire to produce weaker lithosphere but also to reduce the average density of the lithosphere. A persistent reduction in net lithospheric density should reduce the regional depth of the spreading center at scales larger than the flexural wavelengths of the elastic lithosphere. Because the number of seismic measurements of crustal thickness is extremely limited, spreading center depths are sometimes used as a proxy for crustal thickness or thermal structure when no other data are available [e.g. *Klein and Langmuir,* 1987]. The validity of this assumption depends on the compensation of the lithosphere and the importance of dynamic topography at the ridge axis [*Neumann and Forsyth,* 1993]. Seafloor depths increase predictably with age as a result of cooling and thermal contraction [*Parsons and Sclater,* 1977] but flanking and zero-age depths vary considerably on a global basis [*Marty and Cazenave,* 1989]. Since the conductive cooling model does not account for the complexities of ridge axis dynamics, we would not expect thermal subsidence to dominate until the lithosphere has moved some distance away from the spreading center. Some part of the variation in spreading center depth is also expected to be dynamic [e.g. *Sleep and Biehler,* 1970; *Parmentier and Forsyth,* 1985]. It is reasonable to ask whether some part of the variability in regional depth may be related to variations in the thermal and compositional state of the lithosphere and whether these variations are reflected in its deformation. We might therefore expect some global relationship between spreading center depth and near axis roughness.

DETERMINISTIC AND STOCHASTIC SEAFLOOR MORPHOLOGY

Modeling in geodynamics is generally based on deterministic phenomena. This involves measuring a deterministic signal, constructing a physical model to explain it and then finding the parameters of that model

which best describe the observations. This methodology has been used to study phenomena that control the evolution of oceanic lithosphere such as the thermal subsidence [e.g. *Parsons and Sclater,* 1977] and elastic flexure [e.g. *Turcotte,* 1979]. Less attention has been devoted to the understanding of the stochastic component [e.g. *Fox and Hayes,* 1985] although some studies [e.g. *Goff and Jordan,* 1988; *Malinverno and Gilbert,* 1989; *Shaw and Smith,* 1990; *Neumann and Forsyth,* 1995] have developed statistical models to quantify abyssal hill morphology. One objective of this study is to quantify the relationship between the "deterministic" and "stochastic" components of spreading center morphology in order to understand the extent to which the dynamics at the ridge axis influence the stochastic morphology preserved on the flanks. The extent to which the time averaged topography of the flanks can be correlated to the present day axial morphology may provide constraints on the temporal variability of the mechanism(s) of lithospheric deformation.

The expressions deterministic and stochastic are not used here in the strict statistical sense but rather to distinguish between the characteristic components of mid-ocean ridge axial morphology and the smaller scale relief that is superimposed on it. The former is assumed to be a direct manifestation of the deterministic continuum process(es) of lithospheric accretion while the latter is a consequence of the stochastic variations in lithospheric response to the continuum processes. The actual form of the deterministic component at a particular location may eventually be predicted by a physical model whereas the stochastic component can only be described and predicted statistically.

In this analysis, a primary objective will be to separate the characteristic features in the axial morphology from the smaller scale tectonic fabric and quantify the relationship between the two. The across axis bathymetry of the seafloor near a spreading center may thus be envisioned as a sum of a regional mean depth, Z_{avg}, a deterministic component, $\mathcal{D}(x)$, characteristic of all spreading centers and a stochastic component, $S(x)$, unique to that particular location. Specifically, the deterministic component is the characteristic axial rise or axial valley relief and the stochastic component is the collection of individual fault scarps and constructional features that have formed at or near the ridge axis and been transported to the flanks. If these components can be separated then each may be analyzed independently and the relationship between them can be investigated.

EMPIRICAL ORTHOGONAL FUNCTION ANALYSIS

This study uses an Empirical Orthogonal Function (EOF) analysis to quantify axial and flanking morphology in the set of bathymetric profiles described below. The theory of application of EOF's to topographic fields is discussed in detail by *Small* [1994] and will be described only briefly here. The objective of this analysis is to find the components of ridge axis morphology which are common to all spreading centers and to separate these components from those which vary from location to location. The EOF analysis allows us to do this because it decomposes the entire collection of profiles into a common set of independent spatial modes (empirical basis functions) and determines the amount of variance associated with each mode. This variance partition establishes the distinction between the different components of the morphology. It is important to point out that the decomposition upon which the EOF analysis is based is not dependent on any *apriori* assumptions about the structure of the dataset. The spatial modes are eigenvectors of the dataset and are determined subject to the constraint that the maximum amount of variance in the original dataset be described with the smallest number of basis functions possible [*Davis,* 1976].

The EOF decomposition allows an individual bathymetric profile to be described as a linear combination of independent spatial modes (empirical basis functions) as

$$Z_{i0}(x) = \mathbf{c}_{1i}\mathcal{M}_1(x) + \mathbf{c}_{2i}\mathcal{M}_2(x) + \ldots \mathbf{c}_{\mathbf{r}i}\mathcal{M}_r(x) + S_i(x)$$

where

$Z_{i0}(x) = Z_i(x) - Z_{avg}$, is a zero-mean bathymetric profile i, a function of distance x.
$\mathcal{M}_1(x)$, $\mathcal{M}_2(x)...\mathcal{M}_{\mathbf{r}}(x)$ are the spatial modes of the entire dataset.
$\mathbf{c}_{1i}$, $\mathbf{c}_{2i}$ ... $\mathbf{c}_{\mathbf{r}i}$ are the coefficients of the modes for the profile i.
$S_i(x)$ is the linear combination of the remaining modes for profile i.
$\mathbf{r}$ is the number of significant modes.

With this decomposition, any profile may be partially reconstructed as a linear combination of the spatial modes. If we assume that the sum of the significant modes represents the deterministic component of the system then the remainder is stochastic and the representation above reduces to $Z_0(x) = \mathcal{D}(x) + S(x)$. Eigenvalue decompositions have been used investigate deterministic physical processes in dynamical systems with stochastic variability [e.g. *Davis,* 1976; *Priesendorffer,* 1988; *Vautard and Ghil,* 1989]. but here the analysis is limited to decomposition of the dataset. It is beyond the scope of this study to model the deterministic processes responsible for the formation of ridge axis morphology.

The number of significant modes, $\mathbf{r}$, may be inferred from the spectrum of singular values calculated in the analysis. These singular values are the roots of the eigenvalues of the dataset and give the total percentage of variance that is accounted for by each mode. The distribution of variance given by these singular values provides some basis on

which to distinguish between the deterministic and stochastic components of the dataset. In some instances, the dimension of a dynamical system can be estimated by the number of non-zero singular values, each of which corresponds to an eigenfunction of the system [*Vautard and Ghil,* 1989]. The variance related to the stochastic components of the system is distributed over the remaining low-order eigenvectors and the corresponding singular values are smaller but generally non-zero. Because the stochastic component is spatially incoherent from one profile to the next, its variance is distributed over the larger number of low order modes. A clear separation in the size of the singular values allows the components to be distinguished. In this analysis the spectrum of singular values is used to distinguish between the components of the morphology that are consistently present on cross axis profiles from the component which differs from profile to profile.

The representation of ridge axis morphology with EOFs is conceptually similar to the commonly used Fourier representation of geophysical data but has a number of advantages. The spectrum of singular values is analogous to the traditional power spectrum in that both provide estimates of the distribution of variance over a space of basis functions; the difference between the two types of spectra is in the choice of basis functions. A Fourier decomposition represents the signal as a linear combination of analytic sinusoids whereas the EOF decomposition uses empirically determined basis functions. Sinusoids are analytically tractable and offer a natural basis for periodic signals but EOFs are optimum for non-periodic data because they require no assumptions about the form of the basis functions and they are optimized for efficiency rather than analytic tractability. The basis functions used in an EOF analysis are optimum in the sense that they account for as much variance as possible with the smallest number of orthogonal functions. Since periodicity is not built into the basis, no assumptions of statistical stationarity are required in EOF analysis. This is an important factor when dealing with seafloor bathymetry which is generally non-periodic and clearly non-stationary. The EOF decomposition also provides some basis for discriminating between deterministic and stochastic components in the dataset [*Priesendorffer,* 1988; *Vautard and Ghil,* 1989] whereas Fourier analysis of seafloor bathymetry rarely provides an unambiguous spectral separation of these components. The EOF decomposition also allows us to separate the symmetric and antisymmetric parts of the deterministic component of the topography and analyze each separately [*Small,* 1994].

THE DATASET

The analysis presented here is based on a compilation of 228 archival underway profiles (Figure 1) ranging from a PDR record collected in 1959 to Seabeam 2000 centerbeam profiles collected in 1995. Quality control and the logistical requirements of the analysis severely limit the number of usable profiles. In this study, profiles must 1) extend at least 40 km on either side of the ridge axis, 2) cross the axis within 45° of perpendicular, 3) have an average along track sample rate of 1 km or better, and 4) do not intersect known transforms or fracture zones within 40 km of the axis. These requirements were chosen to maximize the number of usable profiles without compromising the resolution of the features that the study seeks to quantify. The basis of this dataset is a set of profiles used in an analysis of axial morphology by *Small* [1994]; the reader is referred to that study for a detailed description of the dataset construction.

This investigation builds upon the analysis of *Small* [1994] but extends the previous study in two ways. First, a considerably larger dataset is used here; the previous study used 156 profiles whereas this study uses 228 profiles. The previous study was limited by a lack of data in many parts of the Southern Ocean - notably the Southeast and Southwest Indian Ridges. Recent surveys of the Southeast Indian Ridge provide continuous coverage of ~2300 km of intermediate spreading rate ridge axis which spans almost the entire global range of axial and flanking morphologies [*Cochran et al,* 1997; *Sempere et al,* 1997]. Also, recent availability of global satellite gravity data [*Sandwell and Smith,* 1997] has allowed the location of many unmapped ridge segments in the Southern Ocean to be determined precisely [*Ludwig and Small,* 1997] so that existing archival profile data may now be used in areas that were poorly understood at the time of the previous study. This has resulted in improved coverage of the Southwest Indian Ridge which is important to constrain the slow end of the spreading rate spectrum. This analysis also includes data from the AAD and Reykjanes Ridge which were not used in the previous study. The second major difference between this and the previous study is that this study focuses specifically on the relationship between axial and flanking morphology whereas the previous study was primarily concerned with variations in axial morphology alone and included only a very limited discussion of the relationship between axial morphology and flanking roughness.

RESULTS AND OBSERVATIONS

Separation of Axial Morphology and Flanking Roughness

The result of the EOF analysis of the 228 profiles is the spectrum of singular values and spatial modes shown in Figure 2. Because the first five singular values are noticeably larger than the others and because the spatial modes corresponding to these five singular values resemble recognizable features of ridge axis morphology, these modes are interpreted as the deterministic component of the dataset. The higher order modes bear no resemblance to ridge axis morphology but rather resemble sinusoids of continuously decreasing wavelength. The first five modes account for 44% of the total variance in the dataset and bear an obvious

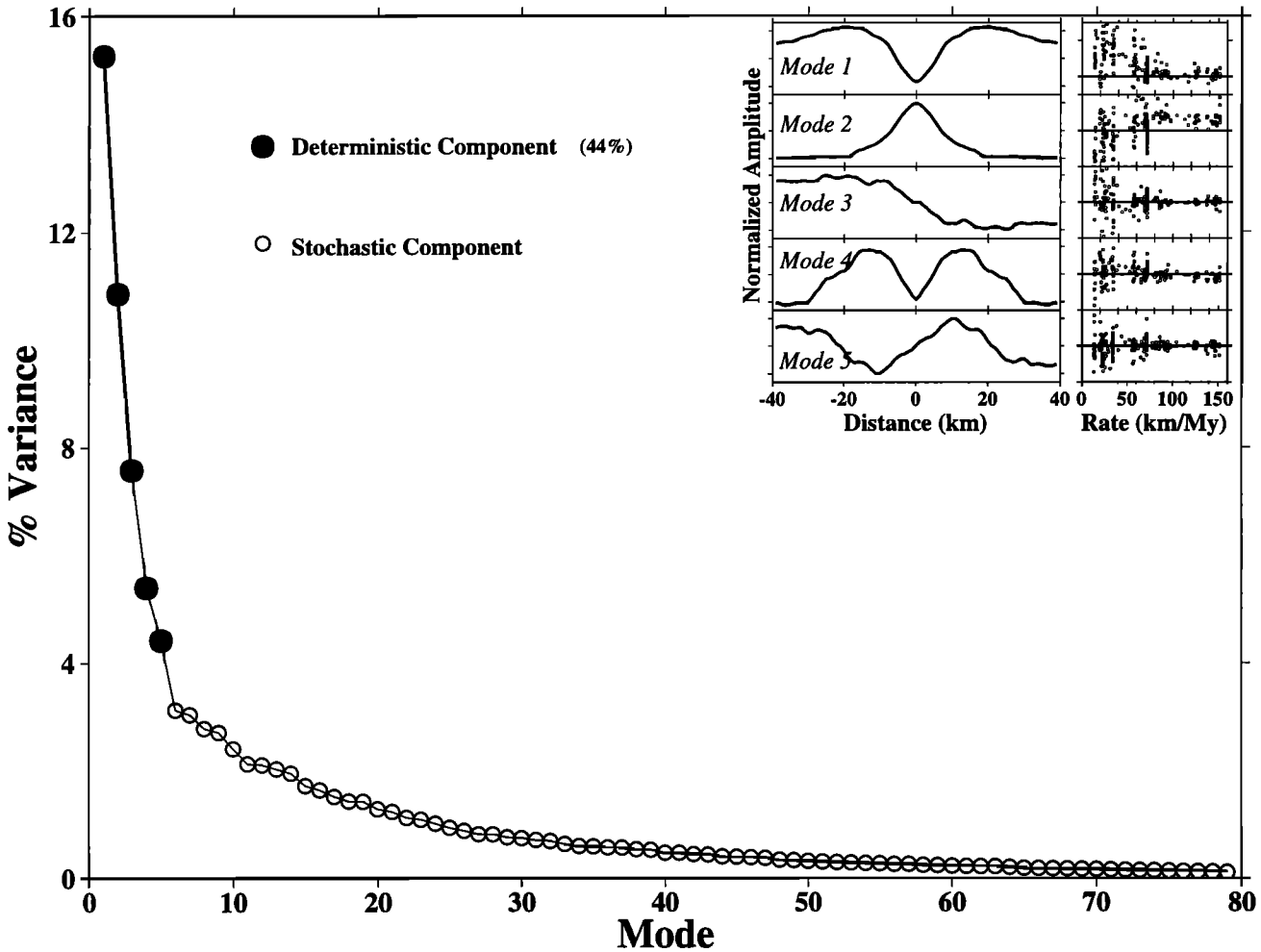

Figure 2. Empirical Orthogonal Function decomposition of the global dataset. The singular values indicate the distribution of variance over the spatial modes given by the decomposition. The spatial modes are common to the entire dataset; the coefficients for each mode correspond to individual profiles. The five largest singular values are interpreted as the deterministic component of the topography and the continuum of smaller singular values represent the stochastic component. The five spatial modes corresponding to the largest singular values and their coefficients for each profile are shown in the insets. These five modes account for 44% of the variance in the dataset.

resemblance to the axial valleys and rises that characterize mid-ocean ridge axial morphology. The component of the topography described by the continuum of higher order modes is considered stochastic and accounts for the remaining variance in the system. Three of the five primary modes are symmetric and two are antisymmetric so it is possible to consider the asymmetry ridge axis morphology separately. The modes estimated from this dataset are effectively identical to those estimated from the subset used by *Small* [1994]. It was shown by *Small* [1994] that the majority of the variance in this system is associated with the high relief of axial valley spreading centers but that the decomposition provides a robust description of the entire dataset. The deterministic component of the each individual profile may be reconstructed as a linear combination of the first five spatial modes as shown in Figure 3. The stochastic component is a linear combination of the remaining modes and forms a residual profile from which the estimates of roughness are derived.

The deterministic and stochastic components of several example profiles are shown in Figure 4. The deterministic component is superimposed on the original bathymetric profile so it is apparent that the basic shape of the axial topography is present in the deterministic component in each

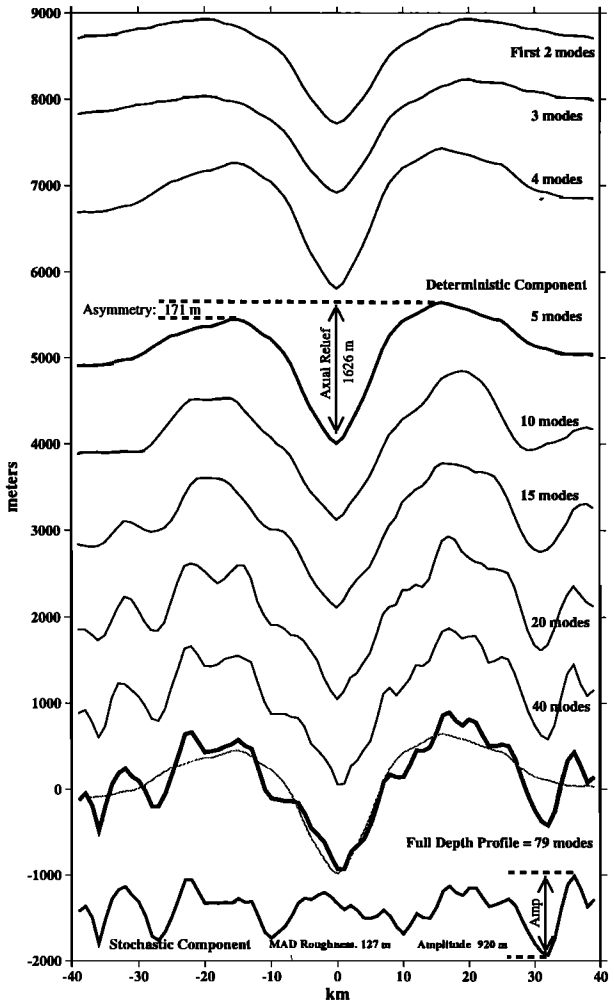

Figure 3. Example of a progressive reconstruction of a single bathymetric profile across the Mid-Atlantic Ridge from its spatial modes. Each plot is a linear combination of an increasing number of the lowest order modes. In the additive model illustrated here, the first five modes are considered the deterministic component of the topography $\mathcal{D}(x)$, the remainder (bottom) forms the stochastic component $S(x)$, and the observed topography is the sum, $Z_0(x) = \mathcal{D}(x) + S(x)$.

case. The residual profiles, shown above each example, illustrate that the variance of the stochastic component of the topography is distributed evenly along the length of the profile and does not result from misfit of the axial morphology. The greatest discrepancy between the bathymetric profile and its deterministic component is seen on some axial rises which are either very narrow or contain a large axial summit caldera. In the case of spreading centers with no discernible axial morphology the deterministic component shows very little relief and almost all of the variance resides in the stochastic component. Two of the profiles across the Reykjanes Ridge have several hundred meter deep grabens superimposed on a broad (60 km) swell. The polarity of the coefficients for these profiles categorize them as axial valleys because the axial swell they are superimposed upon is so broad.

Axial Relief and Width Estimates

A number of parameters can be estimated from the deterministic and stochastic components of each profile. In this study, axial relief is estimated as the range (maximum - minimum) of the deterministic profile; this is always the difference between the center of the axial valley and the higher of the flanks or the difference between the center of the axial rise and the lower of the flanks. Asymmetry is estimated as the range of the asymmetric component of the deterministic profile (mode 3 + mode 5) and is the difference of the flanking depths. The asymmetry values calculated in this study agree closely with those estimated by *Severinghaus and Macdonald* [1988]. The existence of an axial valley or an axial rise may be determined either visually or by the sign of the sum of the coefficients of the symmetric deterministic modes. Axial valley width is measured as the horizontal distance between the shallowest points (maxima) on each side of the deterministic profile.

Roughness Estimates

The statistical characterization of the stochastic topography discussed here is based on the frequency distribution of the roughness profiles derived from the EOF analysis. The dispersion (often called variance) of these profiles as an indicator of the amount of deformation contributed by the processes responsible for the formation of the stochastic component of the topography.

Median Absolute Deviation . One measure of roughness, the Median Absolute Deviation (MAD), is the median of the absolute differences between each point in the residual profile and the median value of the profile [*Rice,* 1988]. The MAD is analogous to the commonly used Root Mean Square (RMS) but is more robust in the presence of extreme values such as those resulting from off axis seamounts. The roughness values computed using this method are very similar to the RMS heights of abyssal hills calculated by *Goff* [1991]. Since the roughness profile provides separate estimates of the stochastic topography on each side of the ridge, the MAD is estimated for each half profile in the dataset. Estimates such as RMS and MAD are indicators of the average variance of the stochastic profile but they consistently underestimate the actual relief of the features that make up the roughness profile (Figure 3). In order to compare the stochastic topography to the

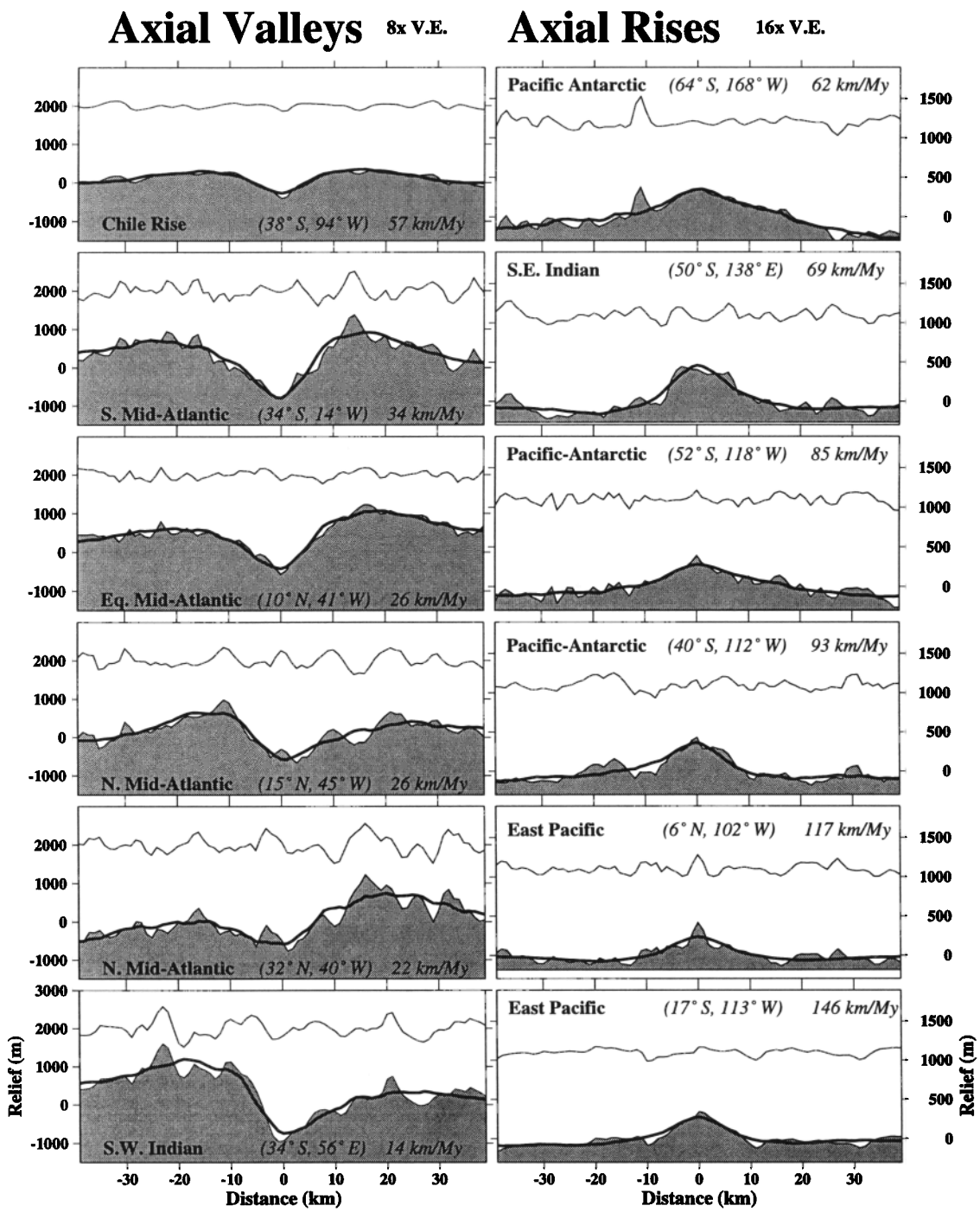

Figure 4. Examples of decomposed profiles for the range of spreading rates and morphologies. The heavy curve is the deterministic component of the topography, $\mathcal{D}(x)$, superimposed on the observed bathymetry $Z_0(x)$. The stochastic component ,$S(x)$, is plotted above each profile. Axial rises and axial valleys are shown at different vertical exaggerations for clarity.

axial topography it is necessary to use an estimate that more accurately reflects the actual relief of the roughness profiles.

Roughness Amplitude. Visual inspection indicates that the extreme (max and min) values on any given stochastic profile are almost always related to one individual feature (Figure 4). These extrema generally appear to be single or nested fault scarps. Although the extrema usually correspond to a single feature, these features are rarely much larger than the other features on the profile. This is reflected by the fact that the frequency distributions of the stochastic profiles are "short tailed". Isolated extrema, such as seamounts, produce long tailed distributions and occur only rarely in this dataset. The extrema may therefore provide an additional estimate of the amplitude of the roughness profile which can be directly compared with the axial relief measurements. It is important however to verify that the extrema are representative of the entire roughness profile.

The difference between the extrema of the stochastic profiles is referred to here as the roughness amplitude. If the stochastic profiles are dominated by short wavelength variance then the amplitude will provide an estimate of the small scale relief generated by the deformation process. The shorter tailed the distribution, the more representative the estimate. A spectral analysis indicates that the majority of the variance in the stochastic profiles occurs at length scales significantly shorter than the half profile length of 40 km. The fact that the stochastic profiles are essentially zero mean (average = 2.2 m) with zero slope (average = 0.2 m/km) supports this observation. Therefore, it is possible to estimate the size of the larger features on the stochastic profile by measuring the difference between the maximum and minimum values of the half profiles. If the profiles are sufficiently short tailed then the extrema are representative of the average relief of the profile. This can be determined using the order statistics of the stochastic profiles. The extrema width is the horizontal distance between the maximum and minimum values of each half profile. Smaller extrema widths support the assertion. The median extrema width for all 456 of the half profiles is 10 km and 83% of the extrema widths are less than 20 km. Only one of the extrema widths longer than 20 km corresponds to a roughness amplitude greater than 1000 m and 75% of the extrema widths longer than 20 km correspond to roughness amplitudes less than 500 m. This suggests that the roughness amplitude of each half profile may provide a reliable estimate of the largest single relief producing feature on each side of the ridge axis. Roughness amplitudes of the half profiles calculated as described above correlate strongly with the MAD roughness estimates (Table 1). Some fraction of the throw of individual faults on the axial valley walls is represented in the relief of the deterministic profile so the roughness amplitudes measured from the stochastic profiles do not represent the actual fault throw. The usefulness of the roughness amplitude is that it provides an additional parameterization of the amplitude of the flanking morphology that may be compared directly with the axial relief measurements.

The roughness estimates discussed here are not necessarily equivalent to abyssal hill topography. Traces of migrating offsets also contribute to the roughness estimates. Without the full two dimensional coverage provided by multibeam data it is not possible to uniquely determine the origin of the stochastic topography. It is important to note however that the MAD roughness estimates of this study are effectively the same amplitude as RMS abyssal hill heights derived from stochastic analyses [*Goff*, 1991, 1992] suggesting that much of the stochastic variability does result from abyssal hills. Some of the profiles included in this analysis cross seamounts but these are isolated features that have a minimal influence on the MAD operator used to estimate roughness from the stochastic profiles. The 1 km sample spacing used in this study is near the limit of resolution for some Pacific abyssal hills but in most cases is adequate to resolve abyssal hill relief. Stochastic analyses [*Goff*, 1991; *Goff et al*, 1995] find that the mean peak to peak characteristic widths of abyssal hills range from 2 km to 14 km but is usually at least 4 km.

In this study roughness is determined only for regions within 40 km of the ridge axis. The majority of this topography presumably results from faulting related to the deformation and migration of lithosphere. Since profiles crossing the ridge at or near first order offsets were eliminated from the dataset, only the scars of smaller propagating offsets should contribute to the roughness discussed here. Using shorter, near axis profiles also eliminates complications related to sedimentation and thermal subsidence. At greater distances from the ridge axis thermal subsidence is the primary component of long wavelength depth variations [*Parsons and Sclater*, 1977] but the high variability in near axis depths (this analysis and [*Marty and Cazenave*, 1989]) suggests that thermal subsidence does not become a dominant factor until the lithosphere has moved some distance away from the ridge. In light of the arguments given above, it is expected that the majority of the stochastic signal discussed here is related to abyssal hill formation with some minor contribution from offset migration and that the contribution from constructional volcanism is negligible.

Global Variations in Axial Relief, Width, Roughness and Depth

Axial relief and asymmetry are plotted as functions of spreading rate in Figure 5. Spreading rates used in this study were calculated with the Nuvel 1a relative plate motion model [*DeMets et al*, 1994] and are given in km/Ma (rather than mm/yr) to better reflect the spatiotemporal resolution of plate velocity estimates. Axial relief and asymmetry in Figure 5 both diminish with increasing spreading rate for axial valleys and are invariant to spreading rate for

Table 1. Correlations and Trends

Parameter 1	Parameter 2	Correlation Coeff.	Rank Order Coeff	Slope	Intercept
Axial Valley Relief	Spreading Rate	0.67	0.61	17.5	-1786
MAD (rise)	Spreading Rate	-0.14	-0.14	----	-----
MAD (valley)	Spreading Rate	-0.67	-0.77	-1.35	165
Log_{10}(MAD (valley))	Log_{10}(Rate)	-0.68	-0.77	-0.50	2.8
Log_{10}(MAD (All))	Log_{10}(Rate)	-0.74	-0.71	-0.63	2.9
Amp. (rise)	Spreading Rate	-0.13	-0.15	----	-----
Amp. (valley)	Spreading Rate	-0.60	-0.70	-7.70	1000
Log_{10}(Amp (valley))	Log_{10}(Rate)	-0.61	-0.70	-0.47	3.5
Log_{10}(Amp (All))	Log_{10}(Rate)	-0.69	-0.67	-0.58	3.6
MAD (rise)	Axial Relief	0.15	-0.04	----	-----
MAD (valley)	Axial Relief	-0.56	-0.64	-0.05	56
MAD (All)	|Axial Relief|	-0.70	0.64	0.06	31
Amp. (rise)	Axial Relief	0.11	0.01	----	-----
Amp. (valley)	Axial Relief	-0.62	-0.66	-0.30	356
Amp. (All)	|Axial Relief|	0.72	0.64	0.38	224
MAD (rise)	Amp.	0.73	0.76	5.14	81
MAD (valley)	Amp.	0.83	0.85	4.82	158
MAD (All)	Amp.	0.89	0.90	5.25	95

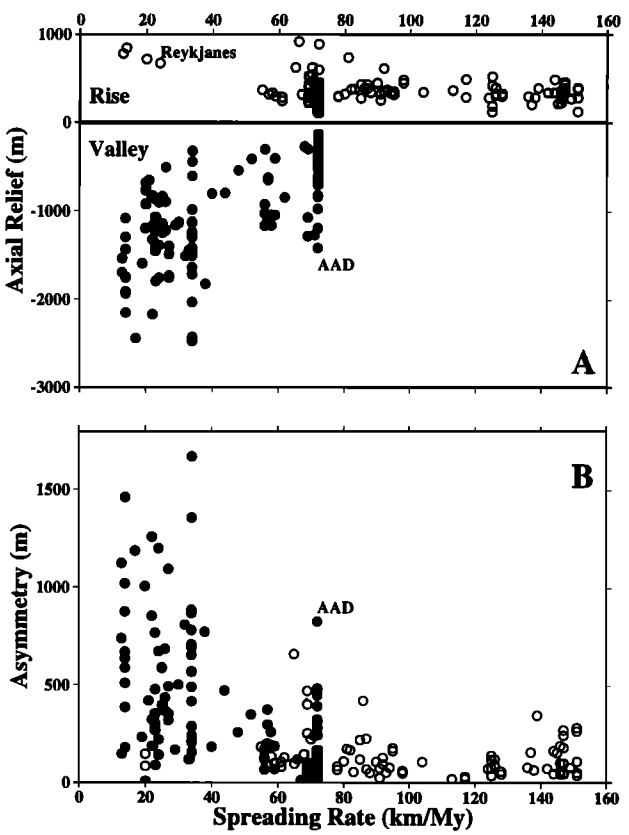

Figure 5. Variation in A) total axial relief and B) asymmetry of axial morphology with spreading rate. Relief and asymmetry of axial valleys diminishes with increasing spreading rate but axial rise relief and asymmetry remains essentially constant over an equivalent range of spreading rates.

axial highs. Both axial relief and asymmetry of axial valleys show considerable scatter and, although the average values diminish with increasing spreading rate, the data show that small (< 1000 m) and symmetric axial valleys are found at all spreading rates between 20 and 75 km/My. The commonly cited dependence of axial valley relief on spreading rate seems less applicable to minimum relief. The presence of the AAD and the relative paucity of mid-ocean ridges with spreading rates between 38 and 60 km/My complicates the interpretation. Axial valley width is relatively uniform (median = 40 km; 50% between 32 and 44 km) and shows no variation with spreading rate.

The variation of both roughness measures with spreading rate (Figure 6) is similar to that of axial relief and asymmetry; a rate dependence for axial valleys with an invariance to spreading rate for profiles characterized by an axial rise. MAD roughness and roughness amplitude are correlated and both show the same variation with spreading rate, thereby supporting the previous assertion that the roughness amplitude is a robust estimate of the average relief of the roughness profile. When plotted in Log_{10} space, the MAD roughness still has considerable scatter and shows a decrease in amplitude with spreading rate for axial valleys but not for axial rises. This observation does not support the continuous power law relationship between roughness and spreading rate proposed by *Malinverno* [1991]

Depth Estimates

Two estimates of spreading center depth are used in this study. Zero-age depth is the single depth value taken at the center of each profile and is identical to the axial depth

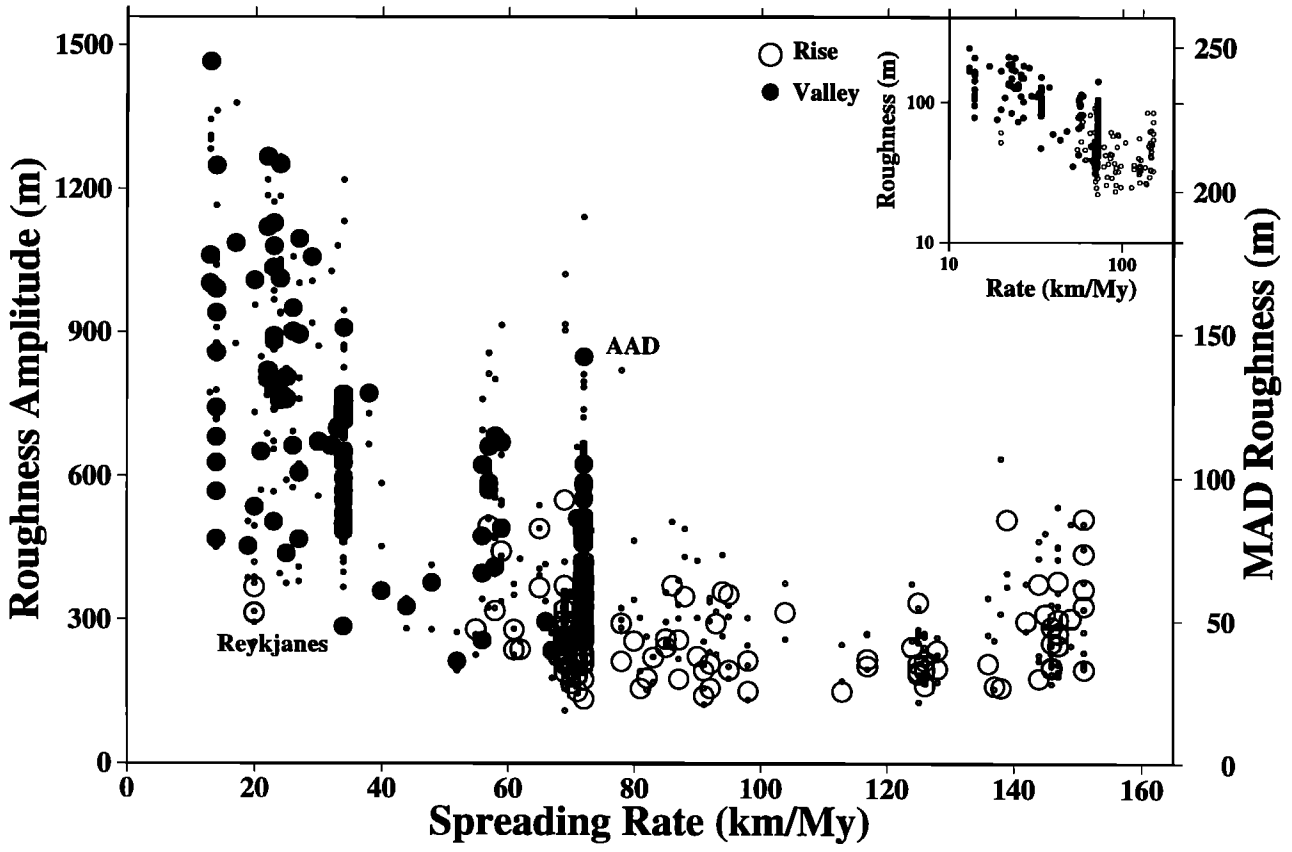

Figure 6. Variation in seafloor roughness with spreading rate. MAD Roughness (large symbols) is the Median Absolute Deviation of the stochastic profile. Roughness amplitude (small symbols) is the maximum relief of the stochastic profile on each side of the ridge axis. Roughness at axial valleys diminishes with increasing spreading rate but minimum values are less dependent on spreading rate. Roughness of axial rise flanking topography is uniformly low and invariant to spreading rate. MAD roughness plotted in Log_{10} space emphasizes the discontinuity between axial valley and axial rise roughness variation and provides little support for a continuous power law model for seafloor roughness.

commonly discussed in studies of mid-ocean ridge segmentation [e.g. *Sempere et al,* 1990]. Profile depth is the arithmetic average of all depth values along the length of a given profile; the median depth along each profile gives nearly the same result. To minimize the influence of the axial morphology, the profile depth can also be estimated as the average depth between distances of 30 and 40 km off axis (Figure 7). Zero-age depth shows a spreading rate variability similar to that of axial relief, asymmetry and roughness. Mean profile depth spans a smaller range and shows greater scatter for profiles with axial valleys than for those with axial rises but otherwise no apparent spreading rate variation.

Correlations

Since this analysis provides estimates of a number of parameters for each profile in the dataset, one way to quantify the relationships between different components of the morphology is to estimate correlations between parameters (Table 1). All correlations are calculated using both the linear correlation coefficient (ρ) and the Spearman rank-order coefficient [*Press et al,* 1992] and generally show close agreement. The correlations provide a convenient way to summarize relationships between the parameters but the results do not generally suggest simple linear relationships between most of the parameters investigated here. In fact, the most significant results of the study may be the lack of correlation and scatter in the relationships between some of the parameters.

It was demonstrated by *Malinverno* [1990] that axial depth and axial valley relief must be correlated since the depth is a component of the relief. It was also shown by *Small* [1994] that the depth of the rift mountains flanking the axial valleys is inversely correlated with axial depth, verifying the common assumption that axial deepening is balanced by flanking uplift. The results of this analysis support the both of these findings and are not shown here.

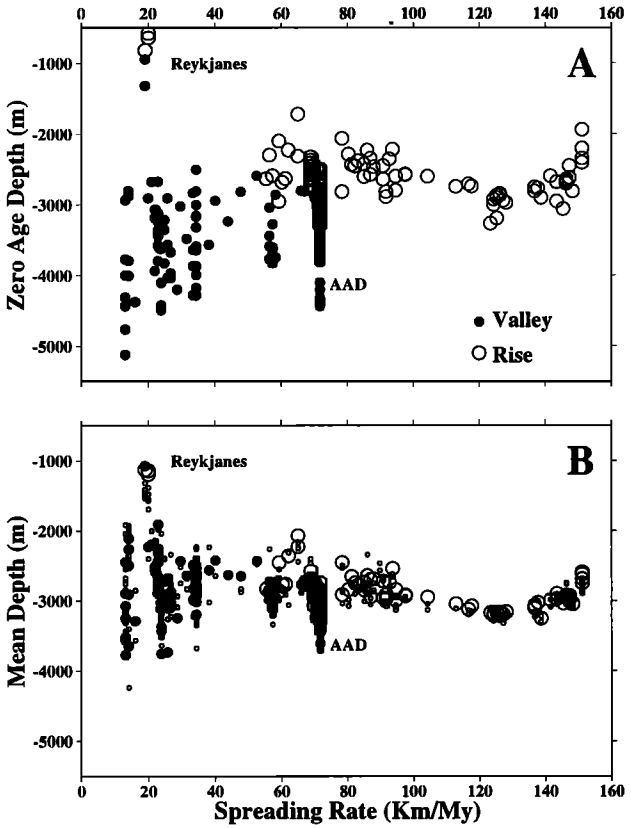

Figure 7. Variation of mid-ocean ridge depths with spreading rate. A) Variation of zero-age depth shows a dichotomy similar to axial relief, asymmetry and roughness. Zero-age depth of axial rises is less variable than that of axial valleys and has no spreading rate dependence. B) Mean spreading center depths within 40 km of the ridge axis have only two thirds the range of zero-age depths and no spreading rate dependence for axial valleys or rises. The greater variability of zero-age depths presumably reflects dynamic topography that is not preserved on the ridge flanks. Mean depths between 30 and 40 km off axis on either ridge flank (small circles) are not influenced by axial topography but show the same pattern. The median spreading center depth for the entire dataset is -2922 m.

The similarity in spreading rate variations of axial relief and roughness suggests a causal relationship. MAD roughness and roughness amplitude are plotted with respect to the axial relief in Figure 8. There are overall correlations (ρ = 0.7) between absolute axial relief and both MAD roughness and roughness amplitude but this is a result of generally lower roughness values for axial rises than for axial valleys. Considered separately, MAD roughness and roughness amplitude are both moderately correlated with axial valley relief (ρ = 0.6) but not with axial rise relief (ρ = 0.1). The same relationship holds true for axial asymmetry. MAD Roughness is also correlated with zero-age depth but this is primarily a result of consistently lower roughness values for axial rises and an overall deepening trend for axial valleys. No correlation (ρ = -0.009) exists between mean profile depth and roughness.

INFERENCES AND IMPLICATIONS

Spreading Center Depth

The variation in zero-age depth with spreading rate is similar to that of axial relief, asymmetry and seafloor roughness but the variation of mean profile depth does not show a similar spreading rate dependence (Figure 7). The global average of profile depths for axial valleys is nearly the same as that of axial rises but the individual profile depths of axial valley spreading centers are more variable, spanning almost twice the 1000 m range of those with axial rises.

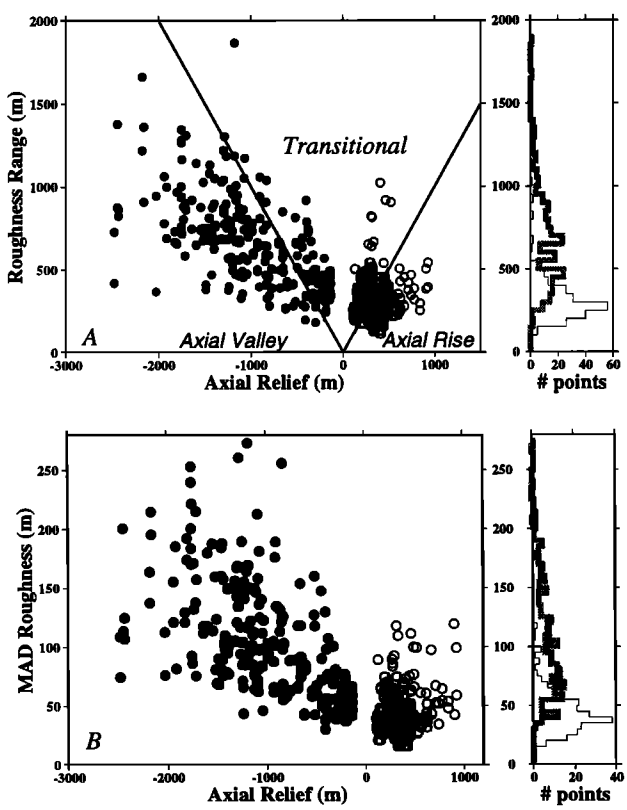

Figure 8. Relationship between roughness and axial relief. Roughness amplitude (A) and MAD roughness (B) are both moderately correlated with axial valley relief but uncorrelated with axial rise relief. Roughness amplitude exceeds axial relief at transitional spreading centers, suggesting that the creation of seafloor roughness does not require significant axial relief. Considerable overlap in axial rise (thin histograms) and axial valley (thick histograms) roughness distributions indicates that the most commonly observed roughness values can be found at either axial rise or axial valley spreading centers, making it difficult to uniquely determine paleo-spreading rate or axial morphology from profile roughness.

Profile depths span only about two thirds the range of zero-age depths which suggests that the remaining third (~1000 m) is dynamically maintained and not preserved once the lithosphere has spread away from the ridge axis. The difference results from dynamic deepening of axial valleys; mean profile depth of axial rise spreading centers is somewhat deeper than zero-age depth but spans essentially the same range. A significant portion of the variation of axial rise profile depths is related to the deepening of the East Pacific Rise in the vicinity of the Galapagos Triple Junction (130 km/My) and shallowing of the robust segment of the Australian-Antarctic Rise adjacent to the Balleny hotspot (65 km/My). The variability of profile depths at any given spreading rate presumably reflects variability in the combined effects of axial dynamics and lithospheric compensation.

A poor correlation (ρ = -0.009) between roughness and profile depth implies that there is no systematic relationship between lithospheric strength and compensation at the scales considered in this study. It is likely that temporal variations in the upwelling patterns of slow spreading ridges result in smaller scale variations in crustal thickness and that their regional influence is limited by the flexural rigidity of the near axis lithosphere. Intrasegment correlations between fault heave and mantle Bouguer anomalies on the Mid-Atlantic Ridge suggest that these variations may occur at spatial scales on the order of ~60 km [*Shaw,* 1992; *Shaw and Lin,* 1993] which is significantly shorter than the estimated flexural wavelength of 100's of kilometers for slow spreading ridges [*Cochan,* 1979; *Forsyth,* 1992]. The lack of global correlation suggests that this may be the case elsewhere.

Seafloor Roughness and Axial Morphology

A significant result of this study is that seafloor roughness near mid-ocean ridges is only moderately correlated with axial valley relief and is not correlated with axial rise relief. Given the similarity in their variation with spreading rate and the long-standing observation that slow spreading centers produce rough topography it is surprising that the actual correlation between axial valley relief and coincident roughness is not stronger. This correlation is weakened by a symmetric dispersion of values about the main trend, corresponding to large valleys with smooth flanks and small valleys with rough flanks. The implication is that roughness and axial valley morphology may be controlled by the same parameters on a global scale but the relief of the axial valley is not the primary determinant of flanking roughness. Alternatively, back rotation and antithetic faulting [*Harrison and Steiltjes,* 1977] may tend to reduce the amplitude of flanking topography at spreading centers with large axial valleys. This would explain some of the scatter in Figure 8 but would not explain the frequent occurrence of rough morphology on the flanks of small axial valleys. Temporal variations in these processes may also weaken the correlation between the instantaneous axial morphology and the time averaged estimate of the roughness. If this were the case however, the limited off-axis extent of the profiles used in this study (< ~2 valley widths) would require that the temporal variations in axial valley relief occur on relatively short time scales. In spite of the moderate correlation of axial valley relief and roughness, the relationship between axial relief and roughness is distinctly different for axial valleys and axial rises (Figure 8). Axial rises show no correlation between the relief of the axial rise and the roughness of the flanking topography.

These results suggest that the variation in roughness with spreading rate is discontinuous and is not necessarily the manifestation of the same mechanism at all spreading centers. The maximum roughness attainable in axial valley environments diminishes with increasing spreading rate and/or thermal structure but the scatter encompasses almost the entire range at any given rate. The latter observation can be explained by intra-segment variability of axial valley spreading centers. The roughness near spreading centers with axial rises shows no significant change with spreading rate (or thermal structure) and is equally variable at all rates. Both the rate dependence and the difference in variability suggest that the mechanism that generates seafloor roughness undergoes a transition coincident with the transition in axial morphology. The Log_{10} plot in Figure 6 emphasizes this discontinuity and does not support the power law dependence on spreading rate proposed by *Malinverno* [1991]. Neither the power law proposed by *Malinverno* [1991] nor the best fit power law for the data in this study (Table 1) adequately describes the roughness variation over the entire range of spreading rates because neither power law flattens sufficiently. As a result, both continuous functions over-predict roughness at intermediate spreading rates and under predict roughness at faster spreading rates. Interestingly, the roughness estimates for axial valleys are fit with exponents of approximately 0.5 when roughnesses from axial rise spreading centers are excluded (Table 1). This is consistent with the notion of a $\sqrt{}$age lithospheric strengthening but the scatter in the roughness estimates (even in Log_{10} space) makes it difficult to draw firm conclusions from the data.

In spite of the discontinuous variation of roughness with spreading rate, it is questionable whether profile roughness can provide accurate estimates of paleo-spreading rates or axial morphologies. The histograms in Figure 8 suggests that very rough seafloor (more than 500 m amplitude) is diagnostic of lower spreading rates but that smoother seafloor (200 - 500 m amplitude) can be generated locally at a wide range of spreading rates and axial morphologies. The considerable scatter limits the inference of paleomorphology to the prediction of an axial valley in the case of anomalously high roughness or an axial rise in the

case of anomalously low roughness. The most commonly observed roughness values (> 50% between 200 and 500 m) are found at all spreading rates. This imperfect correlation between axial valley relief and flanking roughness is also apparent in recent regional multibeam surveys on axial valley and transitional spreading centers. Detailed 2D studies of abyssal hill morphology [eg.*Goff et al,* 1997] may be able to discriminate between seafloor formed at axial rises and axial valleys but it seems unlikely that this will be possible with profile data in heavily sedimented older seafloor.

Transitional Spreading Centers

The relationship between axial valley morphology and roughness undergoes a transition at the point where the amplitude of the roughness exceeds the amplitude of the axial morphology. In these cases the spreading center has little or no distinguishable deterministic axial morphology and neither an axial rise nor valley are evident. Examples of this can be seen in multibeam bathymetry surveys of intermediate rate spreading centers such as the Southeast Indian Ridge [*Cochran et al,* 1997*; Sempere et al,* 1997] and the Pacific Antarctic Rise [*Macario,* 1994; *Macario et al.*, 1994]. Recent studies of the Southeast Indian Ridge have shown that a single segment may contain axial morphologies that range from shallow valleys to small rifted rises [*Cochran et al,* 1997; *Ma and Cochran,* 1996; *Sempere et al,* 1997; *Shah and Sempere,* 1998]. Alternatively, single segments at the same spreading rate may have axial morphology that has neither a rise nor a valley in which the pattern of faulting seen on the flanks is also found at the ridge axis in the absence of any characteristic axial morphology (Figure 9). The abyssal hills formed on the Southeast Indian Ridge also have heights, widths and aspect ratios that span the range between those observed at slower and faster rates [*Goff et al,* 1997]. The characteristics of the segmentation of the Southeast Indian Ridge also vary between the extremes observed at faster and slower spreading rates [*Small et al,* 1998*; Ludwig and Small,* 1997].

Incorporating profiles from the Southeast Indian Ridge into the EOF analysis makes it possible to quantitatively compare transitional morphologies to more thoroughly studied axial rise and axial valley spreading centers. Figure 8a shows that the amplitude of the roughness is significantly less than the relief of the axial valley for valleys larger than 1000 m but for valleys smaller than 500 m the amplitude of the roughness frequently exceeds the relief of the valley. In contrast, at well developed axial rise spreading centers the amplitude of the roughness rarely exceeds the relief of the axial rise by a significant margin. Roughness amplitudes greater than 500 m on axial rise profiles result from seamounts or other isolated features. The majority of the profiles which lie above and between the diagonal lines in Figure 8a correspond to transitional morphologies intermediate between the axial valleys and rises which lie below the diagonals. In the context of the EOF analysis this corresponds to a absence of a characteristic axial morphology and a dominance of the stochastic component. Because the axial relief is estimated by measuring the range of the deterministic component of the topography, this analysis never assigns a exact zero value for axial relief. In some cases, the points which lie above the diagonals in Figure 8 do contain some identifiable axial morphology but the profiles with axial relief estimates less than ~200 m are neither axial valleys nor axial highs and correspond to widely separated extrema on the deterministic profile.

This analysis suggests that the roughness of lithosphere formed at well developed axial rises is lower than that formed at transitional spreading centers without well developed axial morphology. This agrees with the findings of *Goff et al* [1997] in which some abyssal hills on the Southeast Indian Ridge have RMS heights and widths intermediate between those from axial rise and axial valley spreading centers. One possible cause for this further decrease in roughness may be the more frequent occurrence of relief reducing lava flows on magmatically robust axial rise spreading centers [*Macdonald et al,* 1996]. The lack of a steady state magma chamber at intermediate spreading rates may also allow the lithosphere to cool sufficiently to accumulate greater strength and therefore produce larger offset faults than is possible at axial rise spreading centers. The difference in roughness is not large enough however to consistently predict paleo-axial morphology.

The existence of transitional spreading centers with significant topographic roughness but no discernible axial morphology suggests that axial valley relief is not required to generate significant seafloor roughness at intermediate rates (Figure 9). This dataset contains numerous examples where the roughness amplitude exceeds the present axial relief by several hundred meters (Figure 8). This suggests that the roughness is controlled primarily by the extensional strength of the lithosphere and does not rely on deformation related to transport out of a dynamically maintained axial valley. At intermediate spreading rates where an axial rise or valley is not present, the roughness would be a function of the amount of stress that the lithosphere could maintain before faulting and the geometry of the faults produced during failure. Axial morphology also appears to have much greater temporal variability at intermediate spreading rates so the present axial relief may be smaller than that which produced the larger features measured by the roughness amplitude estimate.

In the context of the *Chen and Morgan* [1990*a,b*] model for axial morphology the absence of an axial rise or valley could correspond to a situation in which the axial crust is decoupled from the mantle and is in isostatic equilibrium.

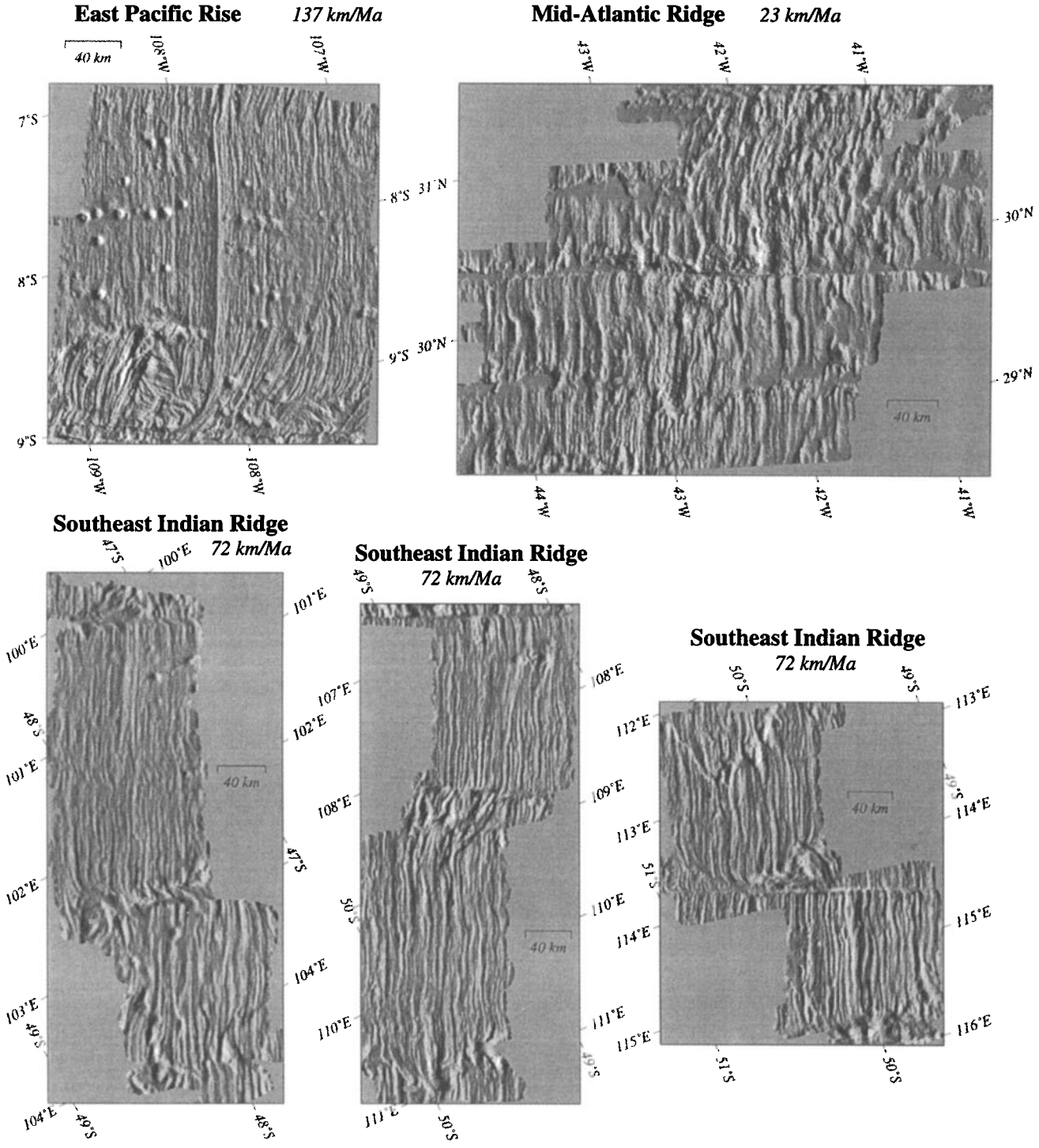

Figure 9. Examples of axial rise, axial valley and transitional spreading center morphologies. Shaded relief images show normalized ridge perpendicular topographic gradients based on multibeam survey data gridded at 500 m resolution. All images are plotted in oblique Mercator projections with the ridge axis vertical. Two dimensional coverage emphasizes the importance of offset propagation to flanking roughness as well as the along axis variability in both axial and flanking morphology. Transitional morphology on the Southeast Indian Ridge shows numerous examples of tectonic fabric formed in the absence of any distinguishable axial morphology. Data were obtained from the RIDGE Multibeam Synthesis (http://www.ldeo.columbia.edu).

Low relief transitional axial morphology could be produced by a temporally variable thermal structure in which the lower crust is weak enough for the system to attain isostatic equilibrium but the mantle is not hot enough to consistently produce an excess of magma and maintain an axial rise.

There exists considerable evidence that the process of abyssal hill formation at axial rises is different from that within axial valleys. Because of the preponderance of steeper inward dipping slopes, normal faulting has long been considered the dominant mode of deformation within axial valleys [*Atwater and Mudie,* 1968; *Searle and Laughton,* 1977; *Macdonald and Atwater,* 1978; *Harrison and Stieltjes,* 1976]. Several authors [e.g. *Dick et al.* 1981; *Karson* 1987; *Brown and Karson,* 1988; *Mutter and Karson,* 1992; *Tucholke and Lin,* 1994; *Goff et al,* 1995] also argue that intrasegment variations in lithospheric strength result in the formation of detachment faults at the ends of axial valley segments which are responsible for much of the lithospheric deformation seen at slow spreading rates. Studies of the intermediate spreading East Pacific Rise [*Normark,* 1976; *Lewis,* 1979], Southeast Indian Ridge [*Sauter et al,* 1991] and Juan de Fuca ridges [*Kappel and Ryan,* 1986] also provide evidence of magmatic and amagmatic episodicity. *Kappel and Ryan* [1986] proposed that abyssal hills on the flanks of the Juan de Fuca Ridge are formed by split axial volcanic ridges which form cyclically and are carried onto the flanks. *Carbotte and Macdonald* [1994] further investigate differences in the morphology of axial rises and propose that those at intermediate spreading centers are volcanic constructs which can be supported by the strength of the lithosphere while the axial highs at fast spreading centers are usually formed on weaker lithosphere and supported isostatically. Stochastic analyses of abyssal hills [*Goff,* 1991; *Goff et al,* 1993] suggest that the size and shape of abyssal hills formed on the East Pacific Rise do not vary significantly with changes in spreading rate but rather with the local segmentation. The results suggest that the dichotomy in axial morphology and the dichotomy in flanking morphology are both controlled by lithospheric strength but that the actual relief of the axial valley is not required to create seafloor roughness.

The Dichotomy in Spreading Center Morphology

The most prominent global characteristic of mid-ocean ridge bathymetric expression is the dichotomy between fast and slow spreading centers. This analysis shows that axial relief, asymmetry, roughness and zero-age depth all have similar variations with spreading rate. For each of these parameters, spreading centers with axial valleys exhibit a variability spanning nearly the full range of each parameter but the maximum attainable value diminishes with increasing spreading rate. This is contrasted by spreading centers characterized by axial rises for which none of these parameters show any significant variation with spreading rate. This pattern suggests that the processes of lithospheric accretion and deformation are controlled by spreading rate or local mantle temperature until a critical rate or thermal structure is attained. Beyond this critical point these processes apparently cease to vary with increasing spreading rate. This type of threshold behavior suggests that the mechanism of lithospheric accretion is characterized by dynamically stable and unstable states which are thermally controlled and generally modulated by spreading rate.

While spreading rate offers a convenient parameterization, it should not be inferred that the rate of plate separation alone is responsible for the pattern seen in these plots. Profiles from the Reykjanes Ridge are more consistent with those of fast spreading ridges and profiles from the AAD are similar to those from slower spreading centers. These "anomalous" spreading centers are the most commonly cited counterexamples suggesting that differences between fast and slow spreading axial morphology are more directly a result of thermal structure. Extensive modeling efforts [e.g. *Sleep,* 1975; *Parmentier,* 1987; *Phipps Morgan et al,* 1987; *Lin and Parmentier,* 1989; *Chen and Morgan,* 1990*a,b*; *Phipps Morgan and Chen,* 1993; *Henstock et al,* 1993; *Neumann and Forsyth,* 1993; *Poliakov and Buck, this volume*] have demonstrated the importance of thermal structure in the formation of axial morphology. Models of lithospheric deformation also demonstrate the importance of thermal structure in the formation of abyssal hill morphology [e.g. *Carbotte and Macdonald,* 1994; *Shaw and Lin,* 1996]. In order to demonstrate a thermal origin for the systematic variations observed in all of these parameters it is necessary to address both the dichotomy in spreading rate dependence and the dichotomy in variability.

Spreading Rate Dependence and Variability of Axial Valley Environments

At a single spreading rate, most of the variability in axial valley relief, asymmetry and roughness results from well known variations in the segmentation of slow spreading plate boundaries. As zero-age depth increases approaching first and second order discontinuities [e.g. *Sempere et al,* 1990] axial valley relief and asymmetry also increase and the roughness of flanking topography tends to increase [*Tucholke and Lin,* 1994]. The deepening of the ridge axis is commonly attributed to an intra-segment variation in mantle temperature and crustal thickness [e.g. *Lin et al,* 1990; *Lin and Phipps Morgan,* 1992] and is accompanied by a corresponding increase in axial relief and asymmetry which may be the result of low angle detachment faulting [*Dick et al.* 1981; *Karson* 1987; *Brown and Karson,* 1988; *Mutter and Karson,* 1992; *Tucholke and Lin,* 1994] or possibly the local stress field [*Severinghaus and Macdonald,* 1988]. Intra-segment variations in abyssal hill morphology on the Mid-Atlantic Ridge also correlate with variations in residual gravity anomalies which are inferred to represent variations in crustal thickness [e.g. *Shaw and Lin,* 1993; *Goff et al,* 1995].

The variability related to segmentation is generally believed to result from temporal and spatial variations in the upwelling of low viscosity asthenosphere [e.g. *Whitehead et al,* 1984; *Schouten et al,* 1985]. The control of upwelling on segmentation may be a result of either shallow redistribution of upwelling material [*Bell and Buck,* 1992; *Wang and Cochran,* 1993] or a transition from 3D to 2D upwelling structure [*Lin and Phipps Morgan,* 1992; *Parmentier and Phipps Morgan;* 1990]. Both mechanisms would depend strongly on thermal structure near the ridge axis. Much of the variability seen in axial valley environments is likely to be related to the episodicity of magmatic and amagmatic extension and the time dependence of mantle upwelling at slower spreading rates and/or colder thermal structures [e.g. *Mutter and Karson,* 1992; *Shaw and Lin,*1993; *Tucholke and Lin,* 1994; *Thatcher and Hill,* 1995]. On a global scale however there appears to be an upper bound on the variability of axial valley environments and this upper bound is presumably related to the thermal structure at the plate boundary.

The results of this study indicate that the average and maximum attainable depth, morphology and roughness of axial valley spreading centers is spreading rate dependent. At any given rate, almost the entire range of any of these parameters is observed. Axial relief and roughness on the Southwest Indian Ridge are not quite as low as those on the faster spreading northern Mid-Atlantic Ridge but the data distribution on the Southwest Indian Ridge is still rather limited. If we assume that the spreading rate dependence of the maxima is thermally controlled then the implication is that it is possible to find almost the entire range of thermal structures at any spreading rate where an axial valley environment can be maintained. Interpreted in the context of the upwelling models discussed above, this would imply that amagmatic extension of strong lithosphere in large, deep axial valleys is thermally controlled by the spreading rate but can be locally overridden by an isolated upwelling of high temperature asthenosphere.

Insensitivity of Axial Rise Environments to Spreading Rate

The variability and spreading rate dependence of slow spreading (10 - 80 km/My) mid-ocean ridges stands in sharp contrast to the relative invariance of axial rise environments to equivalent variations in spreading rate (70-150 km/My). The results of this analysis show no significant variation in axial relief, depth or roughness for axial rise spreading centers. On axial rises, variations in mean depth tend to be regional while variations in axial depth are related to segmentation but neither shows any consistent variation with spreading rate. Detailed analyses of a number of areas on the northern East Pacific Rise indicate that the variability of axial rise spreading centers is controlled by segmentation rather than spreading rate. Cross sectional area of axial rise morphology varies with local segmentation and the presence of an axial magma chamber on the East Pacific Rise but does not show a consistent variation with spreading rate [*Scheirer and Macdonald,* 1993]. Stochastic analyses of abyssal hill morphology on the East Pacific Rise also show consistent variations in height, width and aspect ratio of abyssal hills with ridge axis segmentation but no appreciable spreading rate dependence [*Goff et al,* 1993].

Some aspects of axial rise spreading centers do vary somewhat with increasing spreading rate but this variability is smaller than the intrasegment variation and considerably smaller than the variation seen in axial valley environments. *Carbotte and Macdonald* [1994*b*] show that the relative percentage of inward dipping faults diminishes consistently over the entire range of spreading rates. Limited high resolution deep tow surveys also suggest that throw on abyssal hill bounding faults may decrease somewhat over the range of spreading rates (75 - 150 km/My) on the East Pacific Rise [*S. Carbotte, personal communication*]. Seismic studies indicate that depths to the velocity inversion [*Purdy et al,* 1992] and depths to the top of the magma lens [*Phipps Morgan et al,* 1994] decrease somewhat between rates of 108 and 152 km/My but the uncertainties associated with the former span nearly the same range for both areas.

Spreading Rate Dependence of Internal Structure

The morphologic dichotomy between axial valley spreading centers and axial rise spreading centers is also reflected in a number of other parameters (Figure 10). Mantle Bouguer Anomaly (MBA) amplitudes are characterized by large negative values at axial valley spreading centers and relatively constant higher values at axial rise spreading centers. *Lin and Phipps Morgan* [1991] interpret this pattern as the result of a transition between two and three dimensional upwelling structure as predicted by *Parmentier and Phipps Morgan* [1990]. *Wang and Cochran* [1993] however, find evidence for a localized upwelling structure on the fast spreading East Pacific Rise. Mantle Bouguer anomaly gradients, which normalize for differences in segment length, show a similar global dichotomy between axial rise and axial valley environments. Figure 10 shows the compilation of MBA gradients published by *Wang and Cochran* [1995] supplemented with additional data from the Southeast Indian Ridge [*Cochran et al,* 1996], the AAD [*West and Sempere,* 1998], the Mid-Atlantic Ridge [*Detrick et al,* 1996] and the East Pacific Rise [*Magde et al,* 1996]. Wang and Cochran [1994] interpret this pattern as a result of differences in the mechanism of shallow melt migration and redistribution at fast and slow spreading centers.

Mantle Bouguer anomalies are believed to result from both variations in subaxial mantle temperature and variations in crustal thickness. Seismic estimates of crustal thickness (Figure 10) also show a similar pattern of high variability at low spreading rates and relatively constant values at high spreading rates [*Chen,* 1992]. Regardless of whether these variations in crustal thickness result from differences in the nature of the upwelling structure or from differences in the shallow redistribution of melt and partially

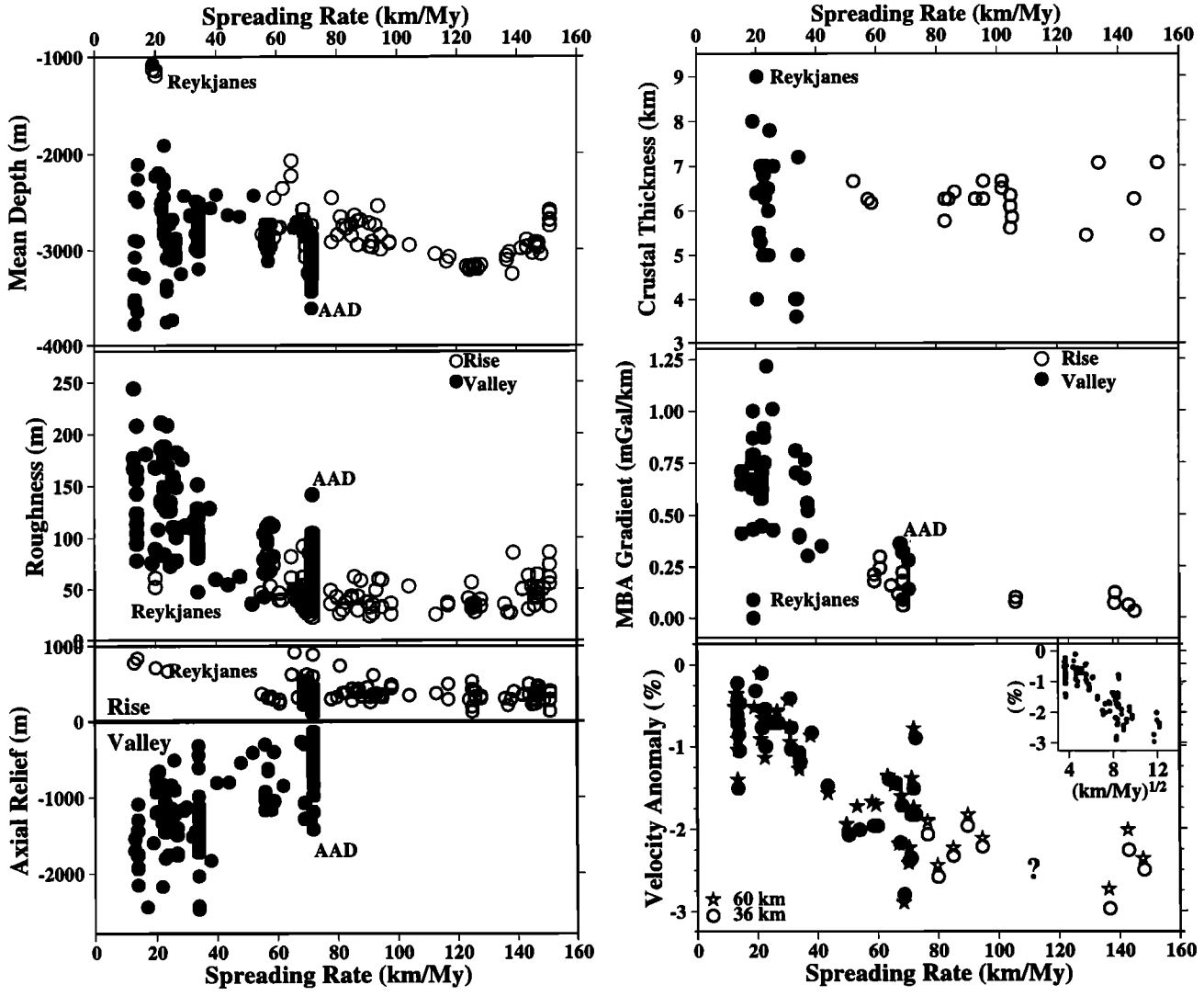

Figure 10. Summary of spreading rate variations of morphologic characteristics estimated in this study and from related studies. Seismically determined crustal thickness [*Chen,* 1990], Mantle Bouguer Anomaly gradient (see text for sources) and seismic velocity anomalies [*Zhang and Tanimoto,* 1993] reveal a dichotomy analogous to that observed in morphology. Variance in crustal thickness and MBA gradients diminishes markedly at higher rates. Velocity anomalies, at depths of 36 and 60 km beneath the ridge axis, show a spreading rate dependence for ridges with axial valleys but no apparent rate dependence for those with axial rises. The inset suggests that the anomalies at the fastest rates are not explained by the lithospheric cooling model. *Zhang and Tanimoto* [1993] did not include data from the EPR between rates of 100 and 140 km/My to avoid hotspot effects.

molten material, the mechanism responsible for these patterns must be strongly temperature dependent and appears to stabilize at intermediate spreading rates.

Global seismic velocity models may provide further support for a stabilization in mid-ocean ridge thermal structure at intermediate spreading rates. Figure 10 shows the results of a global survey of seismic velocity anomalies beneath mid-ocean ridges by *Zhang and Tanimoto* [1993]. These shallow (36 and 60 km) seismic velocity anomalies, estimated from travel time inversion of shear waves and surface waves, show a pattern similar to that seen in the other data discussed above. Travel time delays (relative to the global average) beneath ridges spreading at rates less than ~80 km/My increase with spreading rate but those beneath ridges spreading at faster rates do not continue to increase significantly. Because *Zhang and Tanimoto* [1993] attempted to avoid areas affected by hotspots, a gap in coverage exists between rates of 100 and 140 km/My.

Nonetheless, the seismic velocity anomalies beneath the fastest spreading ridges are essentially the same as those beneath intermediate rate ridges which suggests that doubling the spreading rate does not increase the magnitude of the shallow velocity anomaly at scales resolved by the inversion. We may expect the velocity anomaly to increase linearly with the square root of the spreading rate as a result of the increase in the average lithospheric age within the fixed region about the ridge sampled by the inversion but the inset in Figure 10 suggests that this is not the case for the fast spreading ridges.

The accuracy of Zhang and Tanimoto's velocity model has been questioned by *Su et al* [1992; 1994] but the discrepancy lies at depths greater than 100 km; at shallow depths the model of *Zhang and Tanimoto* [1993] agrees with other global inversions which use different techniques and different seismic phases [see *Su et al*, 1992; 1994]. While the velocity anomalies shown in Figure 10 suggest that regional thermal structure may not change appreciably above intermediate spreading rates, global inversions are limited in resolution and are subject to geographic differences in sampling by teleseismic earthquakes. More detailed studies will be necessary to determine whether the seismic velocity structure of fast spreading centers is actually this insensitive to changes in spreading rate.

Spreading Rate, Stability and Episodicity

The transition between axial rise and axial valley spreading centers occurs within a relatively narrow range of spreading rates where both axial valleys and axial rises occur as well as transitional morphologies that are neither distinct rises nor valleys. The section of the Southeast Indian Ridge between the Amsterdam/Kerguelen hotspots and the AAD shows little change in spreading rate (~72 ± 1 km/My) but the thermal structure of the mantle is believed to have a significant horizontal gradient along axis between the hotspots and the cold region of the AAD [*Roult et al*, 1994; *Sempere et al*, 1997; *West et al*, 1997]. Within this thermal gradient, local perturbations appear to play a major role in local variations in axial and abyssal hill morphology and deformation. The spatial scale of these variations within individual segments suggests that temporal variations between magmatic and amagmatic extension may occur on time scales of less than 10^6 years (Figure 9). The episodicity implied by these spatiotemporal variations does not necessarily require however that the regional thermal structure change significantly at corresponding temporal or spatial scales. The interaction of two or more threshold mechanisms may produce dynamic instability without large changes in the regional thermal structure .

The diversity of morphologies that occur at intermediate spreading rates suggest that the mechanism of lithospheric accretion is easily perturbed and dynamically metastable under the conditions that prevail at intermediate spreading rates. Metastability, marked by vacillation between stable and unstable states, may result from the interaction of various threshold mechanisms such as those proposed for axial morphology [*Chen and Morgan*, 1990*a,b*], magma lens emplacement [*Henstock et al*, 1993; *Phipps Morgan and Chen*, 1993], and mantle upwelling [*Parmentier and Phipps Morgan*, 1990]. Both spatial and temporal variations in thermal structure would exercise a strong control on any of these mechanisms and may account for the diversity of morphologies observed within the transition. Nonlinear coupling between processes of melt production and migration [e.g. *Sparks and Spiegelman*, 1995; *Spiegelman and McKenzie*, 1987] and mechanical deformation [e.g. *Poliakov and Buck, this volume*] may induce episodicity and stability transitions in a manner analogous to that envisioned by *Shaw* [1988] for episodic silicic magmatism. Once the spreading rate increases above a critical point the elevated thermal structure would tend to stabilize the system and maintain a relative steady state in comparison to the strong rate dependence seen at lower spreading rates. The characteristic time scale of the metastable behavior appears to be on the order of 10^5 to 10^6 years for most spreading centers. At time scales longer than 10^6 years, changes in large scale plate motion often have significant effects on the configuration and morphology of the spreading center. At time scales shorter than 10^5 years, the lithosphere is still within the inner valley floor at axial valley spreading centers and has only recently moved beyond the edge of most axial rises at fast spreading centers. The characteristic time scale is presumably controlled by the upwelling rate of buoyant asthenosphere which is responsible for the episodic advection of heat to the ridge axis.

The global dichotomy in variability and spreading rate dependence suggests a stabilization of the mechanism of lithospheric accretion and deformation. This stabilization also appears to be manifest in the low order segmentation of the mid-ocean ridge system [*Ludwig and Small*, 1997]. The coincident transition in axial and flanking morphology and the appearance of a steady state magma chamber further support the assertion that the system has attained a stable configuration. If, as previous work suggests, the processes of lithospheric accretion are controlled primarily by the thermal structure of the spreading center then the implication is that the large scale thermal structure itself does not change appreciably once this transition occurs. To some extent, this can be explained by the asymptotic behavior of most mid-ocean ridge thermal models with spreading rate. Changes in the regional thermal structure are more significant for an incremental rate change at slow spreading rates than they are for an equivalent rate change at fast spreading rates. Asymptotic lithospheric strengthening may therefore be sufficient to explain the overall pattern observed in seafloor roughness but the mechanisms responsible for axial morphology, abyssal hill morphology and segmentation evolution are more complex. The implication of this and numerous other studies is that the

advective-diffusive processes that dictate the thermal structure of mid-ocean ridge systems have inherent stability regimes that control both the formation and deformation of the lithosphere. More detailed studies will be necessary to understand how the mechanisms of accretion and deformation interact to maintain stability and control the morphogenesis of the spreading center.

SUMMARY

Bathymetric measurements at mid-ocean ridges provide information at three different spatial scales: the mean regional depth, the characteristic axial morphology and the smaller scale roughness superimposed on the axial morphology and adjacent flanks. Empirical Orthogonal Function (EOF) analysis of bathymetric profiles across the global mid-ocean ridge system allows these components to be separated and analyzed at coincident locations. The EOF analysis of the 228 profiles in this study provides a basis for a distinction between the deterministic and stochastic components of mid-ocean ridge topography. These results quantify long standing qualitative observations that both axial and flanking morphology vary with spreading rate and allow the relationship between them to be investigated.

The full range of zero-age depths observed at the ridge axis is not preserved on the adjacent ridge flanks. One third of the variation in axial depth appears to be dynamically maintained while the remaining two thirds are preserved on the flanks. Variation in regional spreading center depths decreases with spreading rate for axial valleys but is invariant to spreading rate for axial rises. Regional depth and roughness are uncorrelated so if regional variations in mean depth are a result of crustal thickness and thermal structure this is evidently not reflected in the lithospheric deformation.

At spreading centers with axial valleys the flanking roughness and axial relief diminish with increasing spreading rate. Axial valley relief is moderately correlated with flanking roughness but at intermediate spreading rates the amplitude of the flanking roughness frequently exceeds the relief of the axial valley suggesting that axial relief is not required to form abyssal hills. Distinctive axial morphologies at intermediate spreading rates may be explained by the presence of a weak lower crust that can isostatically decouple the crust and mantle but does not allow sufficient melting to consistently maintain a well developed axial rise. In contrast, spreading centers with axial rises are more sensitive to local segmentation than to spreading rate. Axial relief and flanking roughness are uncorrelated at axial rise spreading centers. Both axial relief and flanking roughness vary discontinuously with spreading rate.

In spite of the discontinuous variation with spreading rate, seafloor roughness does not provide a unique measure of paleo-spreading rate. The presence of anomalously high roughness may be indicative of an axial valley environment but the occurrence of relatively low roughness at almost all spreading rates suggests that it is not generally possible to uniquely determine paleo-axial morphology from profile roughness. Stochastic modeling of two dimensional abyssal hill morphology certainly provides more information about the tectonic environment but it is not straightforward to apply this type of analysis to the older heavily sedimented seafloor.

The most prominent global characteristic of mid-ocean ridge bathymetric expression is the dichotomy between fast and slow spreading centers. This study demonstrates that axial relief, asymmetry, roughness and zero-age depth, as well as several other non-bathymetric observations, all show similar behavior with respect to spreading rate and, presumably, local thermal structure. For each of these parameters, spreading centers with axial valleys exhibit a variability spanning nearly the full range of each parameter but the maximum attainable value diminishes with increasing spreading rate. This is contrasted by spreading centers characterized by axial rises for which none of these parameters show any significant variation with spreading rate. The East Pacific Rise and Pacific Antarctic Rise make up most of the fast spreading part of the system and show a remarkable invariance with spreading rate over more than half the global range of rates (75 - 151 km/My).

The dichotomy in spreading center structure and morphology suggests a transition from episodicity and rate dependence to a more stable mode of accretion. At transitional spreading centers the morphology exhibits even greater sensitivity to small changes in thermal structure. The implication is that the processes of lithospheric accretion and deformation are controlled by spreading rate or local thermal anomalies until a critical point is attained. Beyond this critical point, these processes cease to vary with increasing spreading rate. The most plausible mechanism for such a transition is a stabilization of mid-ocean ridge thermal structure above a critical spreading rate. This type of threshold behavior suggests that the mechanism of lithospheric accretion is characterized by dynamically stable and unstable states which are thermally controlled but generally modulated by spreading rate. The diversity of morphologies that co-exist within a narrow range of intermediate spreading rates further suggest that the mechanism of lithospheric accretion is easily perturbed and is dynamically metastable.

Acknowledgments. The breadth of topics summarized in this paper makes it virtually impossible to acknowledge all the scientists who have contributed to our collective understanding of the subjects. The citations are certainly not exhaustive. I would like to thank Robert Parker, Russ Davis and Alexei Kaplan for sharing their insight into the nuances of EOF analysis and Suzanne Carbotte and John Goff for their insight into the nuances of abyssal hill formation. Conversations with Roger Buck, John Chen, Jim Cochran, Milene Cormier, Dan McKenzie, Alexei Poliakov, Marc Spiegelman and Xuejin Wang also helped to refine the ideas

discussed in this paper. I thank John Goff, Yves Lagabrielle and Dan Scheirer for thorough reviews of the long and tedious manuscript. This research was supported by NSF grant OCE-9302091 and a Lamont-Doherty Postdoctoral Research Fellowship.

REFERENCES

Atwater, T., and J. Mudie, Block faulting on the Gorda Rise, *Science, 159*, 729, 1968.

Batiza, R., Abundances, distribution and sizes of volcanoes in the Pacific Ocean and implications for the origin of non-hotspot volcanoes, *Earth Planet. Sci. Lett., 60*, 195-206, 1982.

Bell, R. E., and W. R. Buck, Crustal control of ridge segmentation inferred from observations of the Reykjanes Ridge, *Nature, 357*, 583-586, 1992.

Brace, W. F., and D. L. Kohlstedt, Limits on lithospheric stress imposed by laboratory experiments, *J. Geophys. Res., 85*, 6248-6252, 1980.

Brown, J. R., and J. A. Karson, Variations in axial processes on the Mid-Atlantic Ridge, *Mar. Geophys. Res., 10*, 109-138, 1988.

Carbotte, S. M., and K. C. Macdonald, The axial topographic high at intermediate and fast spreading ridges, *Earth Planet. Sci. Lett., 128*, 85-97, 1994a.

Carbotte, S. M., and K. C. Macdonald, Comparison of seafloor tectonic fabric at intermediate, fast, and super fast spreading ridges: Influence of spreading rate, plate motions, and ridge segmentation on fault patterns, *J. Geophys. Res., 99*, 13,609-13,631, 1994b.

Carbotte, S. M., S. M. Welch, and K. C. Macdonald, Spreading rates, rift propagation and fracture zone offset histories during the last 5 M.Y. on the Mid-Atlantic Ridge: 25°-27°30'S and 31°-34°30'S, *Mar. Geophys. Res., 13*, 51-80, 1991.

Chen, Y. J., Oceanic crustal thickness versus spreading rate, *Geophys. Res. Lett., 8*, 753-756, 1992.

Chen, Y. J., and W. J. Morgan, Rift valley/no rift valley transition at mid-ocean ridges, *J. Geophys. Res., 95*, 17,571-17,581, 1990a.

Chen, Y. J., and W. J. Morgan, A non-linear rheology model for mid-ocean ridge axis topography, *J. Geophys. Res.*, 95, 17,583-17,604, 1990b.

Cochran, J. R., An analysis of isostasy in the worlds oceans, 2, Mid-ocean ridge crests, *J. Geophys. Res., 84*, 4713-4729, 1979.

Cochran, J. R., J. C. Sempere, D. Christie, M. Eberle, L. Geli, J. A. Goff, H. Kimura, Y. Ma, A. Shah, C. Small, B. Sylvander, B. P. West, and W. Zhang, The Southeast Indian Ridge between 88°E and 120°E: Gravity anomalies and crustal accretion at intermediate spreading rates, *J. Geophys. Res., 102*, p.15506-15520, 1997.

Davis, R. E., Predicatability of sea surface termperature and sea level pressure anomalies over the North Pacific Ocean, *J. Phys. Ocean., 6*, 249-266, 1976.

DeMets, C., R. G. Gordon, D. F. Argus, and S. Stein, Effect of recent revisions to the geomagnetic reversal time scale on estimates of current plate motions., *Geophys. Res. Lett., 21*, 2191-2194, 1994.

Detrick, R. S., H. D. Needham, and V. Renard, Gravity anomalies and crustal thickness variations along the Mid-Atlantic Ridge between 33°N and 40°N, *J. Geophys. Res., 100*, 3767-3787, 1995.

Dick, H. J. B., Low angle faulting and steady state emplacement of plutonic rocks at ridge-transform intersections, *EOS Trans. AGU, 62*, 406, 1981.

Dick, H. J. B., H. Schouten, P. S. Meyer, D. G. Gallo, H. Bergh, R. Tyce, P. Patriat, K. T. M. Johnson, J. Snow, and A. Fisher, Tectonic evolution of the Atlantis II fracture zone, *Proc. Ocean Drill. Program Sci. Results, 118*, 359-398, 1991.

Edwards, M. H., D. J. Fornari, A. Malinverno, and W. B. F. Ryan, The regional tectonic fabric of the East Pacific Rise from 12°50'N to 15°10'N, *J. Geophys. Res., 96*, 7995-8017, 1991.

Epp, D., and N. C. Smoot, Distribution of seamounts in the North Atlantic, *Nature, 337*, 254-257, 1989.

Forsyth, D. W., Comment on "A Quantitative Study of the Topography of the Mid-Atlantic Ridge" by A. Malinverno, *J. Geophys. Res., 96*, 2039-2047, 1991.

Forsyth, D. W., Geophysical constraints on mantle flow and melt generation at mid-ocean ridges. in *Mantle flow and melt generation at mid-ocean ridges*, edited by J.Phipps Morgan and D. Blackman, 1-65, American Geophysical Union, 1992.

Fox, C. G., and D. E. Hayes, Quantitative methods for analyzing the roughness of the seafloor, *Reviews of Geophys. and Space Phys., 23*, 1-48, 1985.

Gente, P., G. Ceuleneer, C. Durand, R. Pockalny, C. Deplus, and M. Maia, Propagation rate of segments along the Mid-Atlantic Ridge between 20 degrees and 24 degrees (SEADMA I Cruise), *Eos, 74n*, 43, 569, 1992.

Grindlay, N. R., P. J. Fox, and K. C. Macdonald, Second order ridge axis discontinuities in the South Atlantic: Morphology, Structure, Evolution, *Mar. Geophys. Res., 13*, 21-49, 1991.

Goff, J. A., A global and regional stochastic analysis of near-ridge abyssal hill morphology, *Jour. Geophys. Res., 96*, 21,713-21,737, 1991.

Goff, J. A., J. R. Cochran, Y. Ma, J.-C. Sempere, and A. Shah, Stochastic analysis of seafloor morphology on the flanks of the Southeast Indian Ridge: The influence of ridge morphology on the formation of abyssal hills, *J. Geophys. Res.,102*, p.15521-15534, 1997.

Goff, J. A., and T. H. Jordan, Stochastic modeling of seafloor morphology: Inversion of Sea Beam data for second-order statistics, *J. Geophys. Res., 93*, 13,589-13,608, 1988.

Goff, J. A., A. Malinverno, D. J. Fornari, and J. R. Cochran, Abyssal hill segmentation: Quantitative analysis of the East Pacific Rise flanks 7°S-9°S, *J. Geophys. Res., 98*, 13,851-13,862, 1993.

Goff, J. A., B. E. Tucholke, J. Lin, G. E. Jaroslow, and M. C. Kleinrock, Quantitative analysis of abyssal hills in the Atlantic Ocean: A correlation between inferred crustal thickness and extensional faulting, *J. Geophys. Res., 100*, 22,509-22,522, 1995.

Harrison, C. G. A., and L. Stieltjes, Faulting within the median valley, *Tectonophysics, 38*, 1377-144, 1977.

Hayes, D. E., and K. A. Kane, The dependence of seafloor

roughness on spreading rate, *Geophys. Res. Lett., 18*, 1425-1428, 1991.

Heezen, B. C., The Rift in the Ocean Floor, *Scientific American, 203*, 99-106, 1960.

Henstock, T. J., A. W. Woods, and R. S. White, The accretion of oceanic crust by episodic sill intrusion, *J. Geophys. Res., 98*, 4131-4161, 1993.

Hey, R. N., A new class of pseudofaults and their bearing on plate tectonics: A propagating rift model, *Earth Planet Sci. Lettr., 37*, 321-325, 1977.

Huang, P. Y., and S. C. Solomon, Centroid depths of mid-ocean earthquakes: dependence on spreading rate, *J. Geophys. Res., 93*, 13445-13477, 1988.

Kappel, E. S., and W. B. F. Ryan, Volcanic episodicity and a non-steady state rift valley along northeast Pacific spreading centers: Evidence from SeaMarc I, *J. Geophys. Res., 91*, 13,925-13,940, 1986.

Karson, J. A., et al, Along axis variations in seafloor spreading in the MARK area, *Nature, 328*, 681-685, 1987.

Klein, E. M., and C. H. Langmuir, Global correlations of ocean ridge basalt chemistry with axial depth and crustal thickness, *J. Geophys. Res., 92*, 8089- 8115, 1987.

LePichon, X., Models and structure of the oceanic crust, *Tectonophysics, 7*, 385-401, 1969.

Lewis, B. T. R., Periodicities in volacanism and logitudnal magma flow on the East Pacific Rise at 23°N, *Geophys. Res. Lett., 6*, 753-756, 1979.

Lin, J., and E. M. Parmentier, Mechanisms of lithospheric extension at mid-ocean ridges, *Geophys. Jour. Int., 96*, 1-22, 1989.

Lin, J., and E. M. Parmentier, A finite amplitude necking model of rifting in brittle lithosphere, *J. Geophys. Res., 95*, 4909-4923, 1990.

Lin, J., and J. Phipps Morgan, The spreading rate dependence of three-dimensional mid-ocean ridge gravity structure, *Geophys. Res. Lett., 19*, 13-16, 1992.

Lin, J., G. M. Purdy, H. Shouten, J. C. Sempere, and C. Zervas, Evidence from gravity data for focused magmatic accretion along the Mid-Atlantic Ridge, *Nature, 344*, 627-632, 1990.

Lonsdale, P. F., Structural geomorphology of a fast-spreading rise crest: The East Pacific Rise near 3°25'S, *Mar. Geophys. Res., 3*, 251-293, 1977.

Ludwig, K., and C. Small, Quantifying large scale mid-ocean ridge segmentation, *Eos, 78*, 46, F682, 1997.

Ma, Y., and J. R. Cochran, Transitions in axial morphology along the Southeast Indian Ridge, *J. Geophys. Res., 101*, 15,849-15,866, 1996.

Macario, A., Crustal accretion at intermediate spreading rates: Pacific-Antarctic ridge at 65°S. Ph.D., Columbia University, 1994.

Macario, A., W. F. Haxby, J. A. Goff, W. B. F. Ryan, S. C. Cande, and C. A. Raymond, Flow line variations in abyssal hill morphology for the Pacific-Antarctic Ridge at 65°S, *J. Geophys. Res., 99*, 17,921-17,934, 1994.

Macdonald, K. C., Mid-ocean ridges: Fine scale tectonic volcanic and hydrothermal processes within the plate boundary zone, *Annu. Rev. Earth Planet. Sci., 10*, 155-190, 1982.

Macdonald, K. C., The crest of the Mid-Atlantic Ridge: Models for crustal generation processes and tectonics. in *The Western North Atlantic Region*, edited by P. Vogt and B. Tucholke, 51-68, Geological Society of America, Boulder, Colo., 1986.

Macdonald, K. C., A new view of the mid-ocean ridge from the behaviour of ridge-axis discontinuities, *Nature, 335*, 217-225, 1988.

Macdonald, K. C., and T. Atwater, Evolution of rifted ocean ridges, *Earth Planet. Sci. Lett., 39*, 319-327, 1978.

Macdonald, K. C., P. J. Fox, R. T. Alexander, R. Pockalny, and P. Gente, Volcanic growth faults and the origin of Pacific abyssal hills, *Nature, 380*, 125-129, 1996.

Macdonald, K. C., R. M. Haymon, S. P. Miller, J. C. Sempere, and P. J. Fox, Deep-Tow and Sea Beam studies of dueling propagating ridges on the East Pacific Rise near 20°40'S, *J. Geophys. Res., 93*, 2875-2898, 1988.

Macdonald, K. C., and B. P. Luyendyk, Investigation of faulting and abyssal hill formation on the flanks of the East Pacific Rise (21°N) using Alvin, *Mar. Geophys. Res., 7*, 515-535, 1985.

Magde, L. S., R. S. Detrick, and the. TERA. group, Crustal and upper mantle contribution to the axial gravity anomaly at the southern East Pacfic Rise, *J. Geophys. Res., 100*, 3747-3766, 1995.

Malinverno, A., A quantitative study of axial topography of the Mid-Atlantic Ridge, *J. Geophys. Res., 95*, 2645-2660, 1990.

Malinverno, A., Inverse square-root dependence of mid-ocean ridge flank roughness on spreading rate, *Nature, 352*, 58-60, 1991.

Malinverno, A., and L. E. Gilbert, A stochastic model for the creation of abyssal hill topography at a slow spreading center, *J. Geophys. Res., 94*, 1665-1675, 1989.

Marks, K. M., and J. M. Stock, Variations in ridge morphology and depth-age relationships on the Pacific-Antarctic ridge, *J. Geophys. Res., 99*, 531-543, 1994.

Marty, J. C., and A. Cazenave, Regional variations in subsidence rate of oceanic plates: a global analysis, *Earth Planet. Sci. Lett., 94*, 301-315, 1989.

McNutt, M., and H. W. Menard, Constraints on yield strength in the oceanic lithopshere derived from observations of flexure, *Geophys. J. R. Astron. Soc., 71*, 363-394, 1982.

Menard, H. W., The East Pacific Rise, *Science, 132*, 1737-1742, 1960.

Menard, H. W., Sea floor spreading, topography and the second layer, *Science, 157*, 923-924, 1967.

Mutter, J. C., and J. A. Karson, Structural processes at slow-spreading ridges, *Science, 257*, 627-634, 1992.

Neumann, G. A., and D. W. Forsyth, The paradox of the axial profile: Isostatic compensation along the axis of the Mid-Atlantic Ridge, *J. Geophys. Res., 98*, 17,891-17,910, 1993.

Neumann, G. A., and D. W. Forsyth, High resolution statistical estimation of seafloor morphology: oblique and orthogonal fabric on the flanks of the Mid-Atlantic Ridge, 34°-35.5°S, *Mar. Geophys. Res., 17*, 221-250, 1995.

Normark, W. R., Delineation of thge main extrusion zone of the East Pacific Rise at latitude 21°N, *Geology, 4*, 681-685, 1976.

Parmentier, E. M., Dynamic topography in rift zones: Implications for lithospheric heating, *Philos. Trans. R. Soc. London. Ser. A, 321*, 23-25, 1987.

Parmentier, E. M., and D. W. Forsyth, Three-dimensional flow beneath a slow spreading ridge axis: A dynamic contribution to the deepening of the median valley toward fracture zones, *J. Geophys. Res., 90*, 678-684, 1985.

Parmentier, E. M., and J. Phipps Morgan, Spreading rate dependence of three-dimensional structure in oceanic spreading centres, *Nature, 348*, 325-328, 1990.

Parsons, B., and J. G. Sclater, Ocean floor bathymetry and heat flow, *J. Geophys. Res., 82*, 803-827, 1977.

Phipps Morgan, J., and Y. J. Chen, The genesis of oceanic crust: magma injection, hydrothermal circulation and crustal flow, *J. Geophys. Res., 98*, 6283-6297, 1993.

Phipps Morgan, J., A. Harding, J. Orcutt, G. Kent, and Y. J. Chen, An observational and theoretical synthesis of magma chamber geometry and crustal genesis along a mid-ocean ridge spreading center. in *Magmatic Systems, edited by M.P. Ryan*, Academic Press, San Diego, CA, 1994.

Phipps Morgan, J., E. M. Parmentier, and J. Lin, Mechanisms for the origin of mid-ocean ridge axial topography: Implications for the thermal and mechanical structure of accreting plate boundaries, *J. Geophys. Res., 92*, 12,823-12,836, 1987.

Poliakov, A.N.B. and W. R. Buck, Mechanics of stretching elastic-plastic-viscous layers: Applications to slow-spreading mid-ocean ridges, *this volume.*

Preisendorfer, R. W., Principal component analysis in meteorology and oceanography. Edited by C.D. Mobley. Amsterdam: Elsevier, 1988.

Press, W. H., B. P. Flannery, S. A. Teukolsky, and W. T. Vetterling, Numerical Recipes. 2 ed. New York: Cambridge University Press, 1992.

Purdy, G. M., L. S. L. Kong, G. L. Christeson, and S. C. Solomon, Relationship between spreading rate and the seismic structure of mid-ocean ridges, *Nature, 355*, 815-817, 1992.

Rice, J., Mathematical Statistics and Data Analysis. Pacific Grove, CA: Wadsworth and Brooks, 1988.

Roult, G., D. Roulland, and J. P. Montagner, Antarctica, II; Upper mantle structure from velocities and anisotropy, *Phys. Earth and Planet.Int., 84*, 33-57, 1994.

Sahabi, M., L. Geli, J. L. Olivet, L. Gilig-Capar, G. Roult, H. Ondreas, P. Beuzart, and D. Aslanian, Moprhological reeorganization with the Pacific-Antarctic Discordance, *Earth Planet. Sci. Lett., 137*, 157-173, 1996.

Sauter, D., H. Whitechurch, M. Munschy, and E. Humler, Periodicity in the accretion process on the Southeast Indian Ridge at 27° 40'S, *Tectonophysics, 195*, 47-64, 1991.

Sandwell, D.T., and W.H.F. Smith, Marine gravity anomaly from Geosat and ERS-1 satellite altimetry, *J. Geophys. Res., 102*, 10,039-54, 1997.

Scheirer, D. S., and K. C. Macdonald, The variation in cross-sectional area of the axial ridge along the East Pacific Rise: Evidence for the magmatic budget of a fast-spreading center, *J. Geophys. Res., 98*, 7871-7885, 1993.

Scheirer, D. S., and K. C. Macdonald, Near-axis seamounts on the flanks of the East Pacific Rise, 8°N to 17°N, *J. Geophys. Res., 100*, 2239-2259, 1995.

Schouten, H., K. D. Klitgord, and J. A. Whitehead, Segmentation of mid-ocean ridges, *Nature, 317*, 225-229, 1985.

Searle, R. C., and A. S. Laughton, Sonar studies of the Mid-Atlantic ridge and Kurchatov fracture zone, *J. Geophys. Res., 82*, 5313-5328, 1977.

Sempere, J. C., J. R. Cochran, D. Christie, M. Eberle, L. Geli, J. A. Goff, H. Kimura, Y. Ma, A. Shah, C. Small, B. Sylvander, B. P. West, and W. Zhang, The Southeast Indian Ridge between 88°E and 120°E: Variations in crustal accretion at constant spreading rate, *J. Geophys. Res, 102*, p.14489-15505, 1997.

Sempere, J. C., G. M. Purdy, and H. Schouten, Segmentation of the Mid-Atlantic Ridge between 24°N and 30°40'N, *Nature, 344*, 427-431, 1990.

Severinghaus, J. P., and K. C. Macdonald, High inside corners at ridge-transform intersections, *Mar. Geophys. Res., 9*, 353-367, 1988.

Shah, A., and J.-C. Sempere, Morphology of the transition from an axial high to an axial valley at the Southeast Indian Ridge and the relation to variations in mantle temperature, *J. Geophys. Res.*, In Press, 1998.

Shaw, H. R., Mathematical attractor theory and plutonic-volcanic episodicity. in Modeling Volcanic Processes, edited by C.Y. King and R. Scarpa, Vieweg, Braunschweig, 1988.

Shaw, P. R., Ridge segmentation, faulting and crustal thickness in the Atlantic, *Nature, 358*, 490-493, 1992.

Shaw, P. R., and J. Lin, Causes and consequences of variations in faulting style at the Mid-Atlantic Ridge, *J. Geophys. Res., 98*, 21839-21851, 1993.

Shaw, P. R., and D. K. Smith, Robust description of statistically heterogeneous seafloor topography through its slope distribution, *J. Geophys. Res., 95*, 8705-8722, 1990.

Shaw, W. J., and J. Lin, Models of ocean ridge lithospheric deformation: Dependence on crustal thickness, spreading rate and segmentation, *J. Geophys. Res., 101*, 17,9777-17,933, 1996.

Sleep, N. H., Formation of oceanic crust: Some thermal constraints, *J. Geophys. Res., 80*, 4037-4042, 1975.

Sleep, N. H., and S. Biehler, Topography and tectonics at the intersections of fracture zones with central rifts, *J. Geophys. Res., 80*, 2748-2752, 1970.

Small, C., A global analysis of mid-ocean ridge axial topography, *Geophys. J. Int., 116*, 64-84, 1994.

Small, C., and D. T. Sandwell, An abrupt change in ridge axis gravity with spreading rate, *J. Geophys. Res., 94*, 17,383-17,392, 1989.

Small, C., D. Sandwell, and J. Y. Royer, Discontinuous geoid roughness along the Southeast Indian Ridge, *Eos, 70*, 15, 468, 1989.

Small, C., J. R. Cochran, J. C. Sempéré and D. Christie, The Structure and Segmentation of the Southeast Indian Ridge, *Marine Geology*, In Press, 1998.

Smith, D. K., and J. R. Cann, The role of seamount volcanism in crustal construction at the Mid-Atlantic Ridge (24°-30°N), *J. Geophys. Res., 97*, 1645-1658, 1992.

Sparks, D., and M. Spiegelman, Self-consistent models of heat and mass transfer between upper mantle and oceanic crust, *Eos, 76n*, 594, 1995.

Spiegelman, M., and D. P. MacKenzie, Simple 2-D models for melt extraction at mid-ocean ridges and island arcs, *Earth Planet. Sci. Lett., 83n*, 137-152, 1987.

Su, W., R. L. Woodward, and A. M. Dziewonski, Deep origin

of mid-ocean ridge seismic velocity anomalies, *Nature, 360*, 149-152, 1992.

Su, W., R. L. Woodward, and A. M. Dziewonski, Degree 12 model of shear velocity heterogeneity in the mantle, *J. Geophys. Res., 99*, 6945-6980, 1994.

Tapponnier, P., and J. Francheteau, Necking of the lithosphere and the mechanics of slowly accreting plate boundaries, *J. Geophys. Res., 83*, 3955-3970, 1978.

Thatcher, W., and D. P. Hill, A simple model for the fault-generated morphology of slow spreading mid-oceanic ridges, *J. Geophys. Res., 100*, 561-570, 1995.

Tucholke, B. E., and J. Lin, A geologic model for the structure of ridge segments in slow-spreading ocean crust, *J. Geophys. Res., 99*, 11,937-11,958, 1994.

Tucholke, B., J. Lin, M. Kleinrock, M. Tivey, T. Reed, J. Goff, and G. Jaroslow, Segmentation and crustal structure of the western Mid-Atlantic Ridge flank, 25 degrees 25'-27 degrees 10'N and 0-29 m.y., *J. Geophys. Res., 102*, 10,203-10,223, 1997.

Turcotte, D. L., Flexure, *Advances in Geophysics, 21*, 51-86, 1979.

Vautard, R., and M. Ghil, Singular spectrum analysis in nonlinear dynamics with applications to paleoclimatic time series, *Physica D, 38*, 395-424, 1989.

Wang, X., and J. R. Cochran, Gravity anomalies, isostasy and mantle flow at the East Pacific Rise crest, *J. Geophys. Res., 98*, 19,505-19,531, 1993.

Wang, X., and J. R. Cochran, Along-axis gravity gradients at mid-ocean ridges: Implications for mantle flow and axis morphology, *Geology, 23*, 29-32, 1995.

West, B. P., W. S. D. Wilcock, and J. C. Sempere, Three-dimensional structure of the asthenospheric flow benearh the Souteast Indian Ridge, *J. Geophys. Res., 102*, 7783-7802, 1997.

West, B. P., and J. C. Sempere, Gravity anomalies, flexure of axial lithosphere, and along-axis asthenospheric flow beneath the Southeast Indian Ridge, *Earth Planet. Sci. Lett.*, In Press, 1998.

Whitehead, J., H. J. B. Dick, and H. Schouten, A mechanism for magmatic accretion under spreading centres, *Nature, 312*, 146-148, 1984.

Zhang, Y. S., and T. Tanimoto, High resolution global upper mantle structure and plate tectonics, *J. Geophys. Res., 98*, 9793-9823, 1993.

C. Small, Lamont-Doherty Earth Observatory, Palisades, NY 10964, (email, small@ldeo.columbia.edu)